Synaptic modulation mediated by the endocannabinoid 2-arachidonoylglycerol in the central nervous system.

（中枢神経系における内因性カンナビノイド2- アラキドノイルグリセロールによるシナプス修飾）

谷村あさみ

CONTENTS

Abstruct

Endocannabinoids are released from postsynaptic neurons and cause retrograde suppression of synaptic transmission. Anandamide and 2-arachidonoylglycerol (2-AG) are regarded as two major endocannabinoids. To determine to what extent 2-AG contributes to retrograde signaling, I analyzed mutant mice lacking either of the two 2-AG synthesizing enzymes diacylglycerol lipase α (DGLα) and β (DGLβ). Endocannabinoid-mediated retrograde synaptic suppression was totally absent in the cerebellum, hippocampus and striatum of DGLα knockout mice, whereas the retrograde suppression was intact in DGLβ knockout brains. These results clearly indicate that 2-AG produced by DGLα, not by DGLβ, mediates retrograde synaptic suppression.

To elucidate how 2-AG signaling is terminated after inducing retrograde synaptic suppression, I examined the cerebellum of mice lacking the 2-AG hydrolyzing enzyme monoacylglycerol lipase (MGL) or mice with cerebellar granule cell (GC)-specific deletion of MGL. In wild-type cerebellum, MGL was expressed richly in terminals of parallel fibers (PFs), the axons of GCs, and weakly in Bergman glia (BG), but was absent in climbing fiber (CF) terminals and GABAergic terminals. Despite this highly selective MGL expression pattern, 2-AG-mediated retrograde suppression was

significantly prolonged at not only PF-Purkinje cell (PC) synapses but also CF-PC synapses in GC-specific MGL knockout mice. Virus-mediated expression of MGL into BG of global MGL-KO mice significantly shortened 2-AG-mediated retrograde suppression at PF-PC synapses. Furthermore, contribution of MGL to termination of 2-AG signaling depended on the distance from MGL-rich PFs to inhibitory synaptic terminals. These results indicate that 2-AG is degraded in a synapse type-independent manner by MGL present in PFs and BG.

General introduction

Marijuana refined from *cannabis sativa* induces various psychotropic actions such as hallucination, analgesia, increased appetite, motility disturbance. Δ^9 tetrahydrocannabinol (Δ^9-THC) (Figure 1) was identified as the major psychoactive component of cannabis in 1964 (1). In 1990s, two types of receptors that bind Δ^9-THC were cloned and named cannabinoid CB_1 (CB_1R) and CB_2 receptors (CB_2R) (2, 3). Meanwhile, molecules that are synthesized *in vivo* and can activate cannabinoid receptors are searched. Then, *N*-arachidonylethanolamide (anandamide) and 2-arachidonylglycerol (2-AG) were identified as major endocannabinoids, i.e., the endogenous ligands for cannabinoid receptor (4-6).

In 1991, it was reported that strong depolarization of cerebellar Purkinje cells (PCs) suppressed GABA release from inhibitory synaptic terminals (7). This suppression was blocked by inhibiting the elevation of intracellular Ca^{2+} concentration in postsynaptic PCs, indicating that the suppression of GABA release requires a retrograde messenger released from postsynaptic PCs. It took 10 years for researchers to identify the retrograde messenger for depolarization-induced suppression of transmitter release. In 2001, three groups reported at the same time that endocannabinoids mediate the

retrograde signaling (8-10). Since then, numerous studies have been performed to understand the mechanisms and physiological roles of endocannabinod-mediated retrograde modulation of synaptic transmission.

Cannabinoid receptors and endocannabinoid

Cannabinoid receptors consist of two isoforms and both are seven-transmembrane-domain receptors coupled to $G_{i/o}$ protein. While type 1 cannabinoid receptor (CB_1) is richly expressed in the brain and spinal cord, type 2 cannabinoid receptor (CB_2) is expressed in the immune system of periphery. CB_1 receptors are located in axons and presynaptic terminals throughout the brain and spinal cord (11). Activation of CB_1 receptor inhibits adenylyl cyclase or cAMP production and modulates various types of ion channels and enzymes in a cAMP-dependent or -independent manner. Stimulation of CB_1 receptor induces activation of A-type (12) and inwardly rectifying K^+ channels (13) and inhibits N- and P/Q-type Ca^{2+} channels (14) and D- and M-type K^+ channels (15, 16).

Anandamide (AEA) (4) and 2-arachidonoylglycerol (2-AG) (5, 6) are condidered to be two major endocannabinoids. These are lipid in nature and produced from arachidonic acid-containing membrane lipids. AEA and 2-AG has different structures

(Figure 1), different biosynthesis and degradation pathways (Figure 2). Biochemical pathways for AEA formation have been investigated extensively but still not fully understood. It was reported that AEA is produced from phospholipids through two enzymatic reactions, *N*-acyltransferase and *N*-acylphosphatidylethanolamine-hydrolyzing phospholipase D (NAPE-PLD) (17). However, NAPE-PLD knockout mice can produce AEA in an NAPE-PLD dependent manner (18). This finding suggests that AEA is synthesized by another pathway *in vivo*. AEA is known to be catalyzed by fatty acid amide hydrolase (FAAH) into arachidonic acid and ethanolamine. 2-AG is generated also by two enzymatic reactions through phospholipase C (PLC) and diacylglycerol lipase (DGL) (11). 2-AG is hydrolyzed into arachidonic acid and glycerol mostly by monoacylglucerol lipase (MGL). A study using a functional proteomic strategy demonstrates that MGL accounted for approximately 85 % of 2-AG hydrolysis and that the remaining 15 % is catalyzed by other enzymes, such as ABHD6 and ABHD12 (19). Duration and extent of endocannabinoid-meidated signaling are dependent on the balance between production and degradation of endocannabinoids.

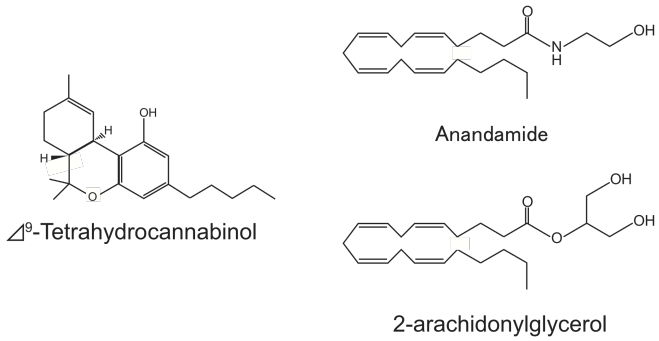

Figure 1. Structural formula of Δ9-tetrahydrocannabinol and major endocannabinoids.

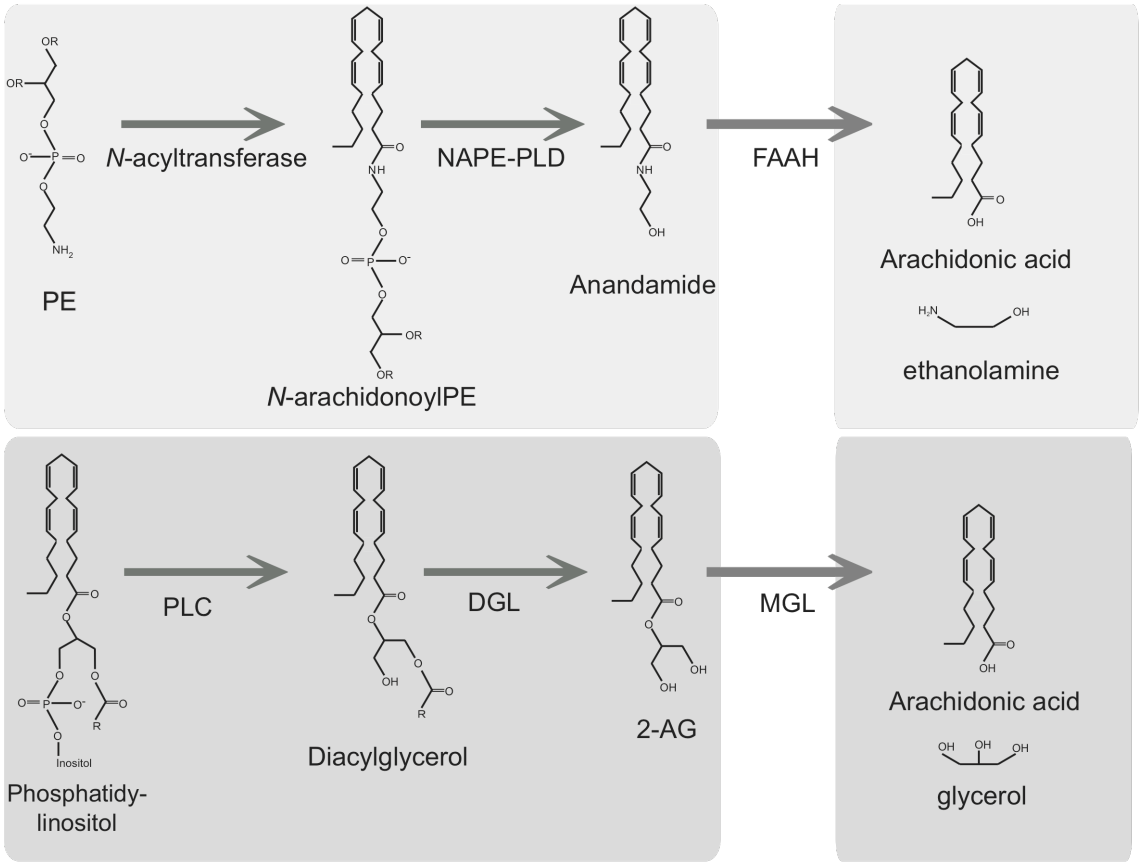

Figure 2. Production and degradation of endocannabinoid.

Anandamide is produced from phosphatidyl ethanolamine (PE) by tow enzymatic steps and is degradated by fatty acid amide hydrolase (FAAH). NAPE-PLD: N-acylphosphatidylethanolamine-hydrolyzing phospholipase D

2-arachidonylglycerol (2-AG) is produced from phosphatidylinositol via phospholipase C (PLC) and diacylglycerol lipase (DGL). Monoacylglycerol (MGL) hydrolyzes 2-AG.

Endocannabinoid-mediated retrograde signaling

A major physiological role of endocannabinoids is to mediate retrograde signaling at synapses. Endocannabinoids are produced and released from postsynaptic neurons in activity dependent manners, travel retrogradely across the synaptic cleft, and bind to CB_1 receptors at presynaptic terminals. Activation of presynaptic CB_1 receptors leads to suppression of neurotransmitter release including glutamate, GABA and glycine. As for endocannabinoid production and release from neurons, three distinct mechanisms have been identified (Figure 3).

1) Ca^{2+}-driven endocannabinoid release (Ca^{2+}-driven ER)

A large postsynaptic Ca^{2+} elevation alone can trigger endocannabinoid production and release. Strong depolarization of postsynaptic neurons induces Ca^{2+} influx through voltage-gated calcium channels. Eleveation of intracellular Ca^{2+} level to micro-molar range releases endocannabinoids that act retrogradely onto presynaptic CB_1 receptors and transiently suppress the release of GABA or glutamate. This phenomenon is termed depolarization-induced suppression of inhibition (DSI, for the suppression of GABA) or excitation (DSE, for the suppression of glutamate). How Ca^{2+} elevation induces endocannabinoid production and release remains unclear. Ca^{2+} influx through NMDA

receptors can also induce endocannabinoid release and retrograde suppression in cultured hippocampal neurons (20).

2) Receptor-driven endocannabinoid release (RER)

Production and release of endocannabinoid are induced by activation of $G_{q/11}$-coupled receptors at basal intracellular Ca^{2+} level. The receptors that can trigger endocannabinoid release include group 1 metabotropic glutamate receptors (mGluRs) (21), M_1/M_3 muscarinic receptors (22), 5-HT_2-type serotonin receptors (5-HT_2R) (23), orexin receptors (24) and oxytocin receptors (25). Strong activation of these $G_{q/11}$-coupled receptors induces production of 2-AG in a Ca^{2+}-independent manner through the action of PLCβ and DGL.

3) Ca^{2+}-assisted receptor-driven endocannabinoid release (Ca^{2+}-assisted RER)

2-AG is produced and released from neurons when weak depolarization that is subthreshold for Ca^{2+}-driven ER is combined with weak $G_{q/11}$-coupled receptor activation that is also subthreshold for RER (26-29). This phenomenon is considered to result from the activation property of PLCβ. Activity of this enzyme has been shown to depend on both $G_{q/11}$-coupled receptor activation and intracellular Ca^{2+} level (25). Hence, PLCβ can function as a coincidence detector of $G_{q/11}$-coupled receptor activation (that

reflects amount of transmitter released from presynaptic terminals) and postsynaptic Ca^{2+} level (that reflects activity of postsynaptic neurons).

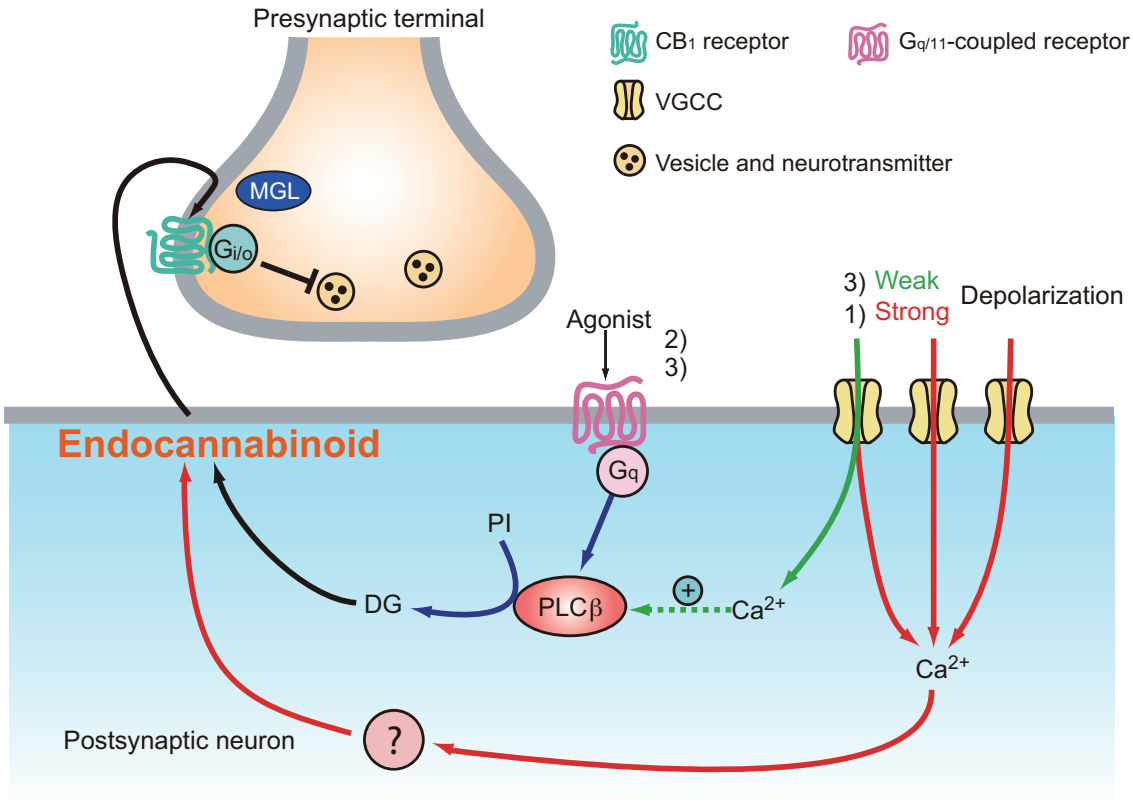

Figure 3. Molecular mechanisms of endocannabinoid-mediated retrograde suppression

1) Elevation of intracelluar Ca^{2+} concentration induced by strong depolarization.

2) Activation of postsynaptic $G_{q/11}$-coupled receptors and phospholipase Cβ (PLCβ).

3) Combination of weak depolarization and weak activation of $G_{q/11}$-coupled receptors.

PI: phosphatidylinositol, DG: diacylglycerol

Part 1

Introduction

Endocannabinoids are released from postsynaptic neurons and cause retrograde suppression of synaptic transmission through activation of CB_1 receptor. Endocannabinoid –mediated retrograde suppression is induced by Ca^{2+}-driven ER, strong activation of $G_{q/11}$- coupled receptors at basal intracellular Ca^{2+} level (RER), or Ca^{2+}-assisted RER.

AEA and 2-AG have been regarded as two major endocannabinoids. AEA is produced from phospholipids through two enzymatic reactions, *N*-acyltransferase and PLD. 2-AG is generated by combination of membrane PLC and DGL. The first step is hydrolysis of arachidonic acid-containing membrane phospholipid. Then, 2-AG is generated from arachidonic acid-containing DG produced at first step by the action of DGL.

Pharmacological data suggest that 2-AG function as a retrograde messenger at synapse in various regions of the central nervous system (CNS) (11). Inhibitors of DGL have been reported to block RER(24, 27, 30-33). In contrast, there are a number of reports as to the effects of DGL inhibitors on Ca^{2+}-driven ER, but the results are controversial (33-36). I could not draw a conclusion that AEA or 2-AG which is major retrograde messenger. Such inconsistent results may depend on different methods of

pharmacological experiments.

Two closely related genes encoding DGL activity were cloned and named DGLα and DGLβ (37) . Experiments with overexpression of DGLα (37) and those with pharmacological blockade or knockdown of endogenous DGLα/β by RNA interference (31, 37) indicate that DGLα and/or DGLβ are major 2-AG synthesizing enzymes. To determine to what extent 2-AG mediates retrograde signaling and to clarify the relative contributions of DGLα and DGLβ in 2-AG biosynthesis, I generated mutant mouse lines lacking either of the two DGL isoforms.

By analyzing these knockout mice, I demonstrate that 2-AG produced by DGLα, not by DGLβ, is a ubiquitous retrograde messenger at central synapses.

Materials and Methods

Production of DGLα and DGLβ knockout mice

DGLα knockout mice were produced by homologous recombination using the ES cell line RENKA, which I developed from the C57BL/6N strain (38). A targeting vector constructed in accordance with the mouse genomic DNA databases contained exon 3 and 4 of *Dagla* gene with the 3.7 kb upstream and 5.8 kb downstream homologous genomic DNA fragments and the diphtheria toxin gene for negative selection (Figure 4A). A DNA fragment, which carried a 34 bp loxP sequence and pgk-1 promoter-driven neomycin phosphotransferase gene (pgk-neo) flanked by two Flp recognition target (*frt*) sites, was inserted into the site 100 bp upstream of the exon 3. The other loxP site was introduced into the site 207 bp downstream of the exon 4 in order to eliminate the exon 3 and 4 containing the two putative transmembrane domains (37) after Cre-loxP deletion. This resulted in a frame-shift mutation in the *Dagla* gene (Figure 4A).

Homologous recombination in the ES cells and chimeric mice production were carried out as described previously (38). Resulting chimeric mice were mated with C57BL/6 mice, and offspring ($Dagla^{+/lox(neo)}$) were further crossed with *TLCN-Cre* mice (39) to delete the exon 3 and 4 of *Dagla* gene and neo cassette. The Cre gene was bred

out in the next generation. After confirming deletion of the neo cassette and the exon 3 and 4, heterozygous (Daglα$^{+/-}$) mice were mated to generate homozygous (Daglα$^{-/-}$) mice (Figure 4C). Western blot analysis of cerebellar homogenate samples confirmed the absence of DGLα signals in α-KO mice. Genotypes for all subsequent breedings were determined by PCR analysis of digested mice tail samples (Figure 4C). PCR genotyping of mice tail DNA was performed with the following primers: forward, 5'-GTCTGACTCCAGAGCTCTTG-3'; reverse, 5'-GAACTTGCTGTGTACACTAG -3'.

DGLβ knockout mice were produced also by homologous recombination using the ES cell line RENKA. The targeting vector included exon 10 and 11 of *Daglb* gene containing one of the two putative catalytic triad, serine (37) with the 5.13 kb upstream and 5.7 kb downstream homologous genomic DNA fragments and the diphtheria toxin gene for negative selection (Figure 4B). The DNA fragment, which carried the loxP sequence and pgk-neo casette, was inserted into the site 260 bp upstream of the exon 10. The other loxP site was introduced into the site 170 bp downstream of the exon 11 (Figure 4B). Floxed mice (Daglβ$^{+/lox(neo)}$) were established from the homologous recombinant clones. DGLβ knockout mice were produced by crossing DGLβ floxed

mice and *TLCN-Cre* mice (Figure 4E). Northern blot analysis of total RNA samples from forebrain and cerebellum confirmed the absence of DGLβ mRNA in β-KO mice (Figure 4F). Genotypes for all subsequent breedings were determined by PCR analysis of digested mice tail samples with the following primers: forward, 5'-GCTTGTCCAGATGCACAAGA-3'; reverse, 5'-TCATTTAGCCAGGATCACAG-3'.

Recordings from cerebellar slices

Parasagittal slices (250 μm thick) from the cerebellar vermis were prepared from mice aged 23 to 60 postnatally (for studying PF-mediated EPSCs in PCs) or juvenile mice at P8 to P18 (for CF-mediated EPSCs and IPSCs in PCs and PF-mediated EPSCs in INs) (40). The standard external solution contained (in mM) 125 NaCl, 2.5 KCl, 2 $CaCl_2$, 1 $MgSO_4$, 1.25 NaH_2PO_4, 26 $NaHCO_3$, and 20 glucose, bubbled with 95% O_2 and 5% CO_2 (pH 7.4). A recording chamber was perfused with the external solution supplemented with 10 μM bicuculline or 100 μM picrotoxin (for recording EPSCs), or with 10 μM 2,3-Dioxo-6-nitro-1,2,3,4-tetrahydrobenzo quinoxaline-7-sulfonamide (NBQX) (for recording IPSCs).

Whole-cell recordings were made from visually identified PCs or INs at 32 ºC using

an upright microscope (BX50WI; Olympus, Tokyo, Japan) equipped with an IR-CCD camera system (Hamamatsu Photonics, Hamamatsu, Japan) (28). Patch pipettes (2-4 MΩ) were filled with one of the solutions with the following compositions (in mM). (1) 140 CsCl、1 EGTA、10 HEPES、 4.6 $MgCl_2$、0.1 $CaCl_2$、4 Na_2ATP、 0.4 Na_2GTP (pH 7.3, adjusted with CsOH) for the DSE experiments. (2) 30 CsCl、110 D-gluconate、1 EGTA、10 HEPES、4.6 $MgCl_2$、0.1 $CaCl_2$、4 Na_2ATP、0.4 Na_2GTP (pH 7.3, adjusted with CsOH) for the DSI experiments. (3) 60 CsCl、10 D-gluconate、20 TEA-Cl、 30 HEPES、20 BAPTA-4K、4 $MgCl_2$、4 Na_2ATP、0.4 Na_2GTP (pH 7.3, adjusted with CsOH) for the experiments of mGluR1 agonist-induced retrograde suppression. (4) 130 K D-gluconate, 6 KCl, 10 NaCl, 10 HEPES, 0.16 $CaCl_2$, 2 $MgCl_2$, 0.5 EGTA, 4 Na-ATP and 0.4 Na-GTP (pH 7.3, adjusted with KOH) for the experiments of PF-induced retrograde suppression. Membrane currents were recorded with an EPC-9/2 amplifier (HEKA Elektronik, Lambrecht/Pfalz, Germany). The signals were filtered at 3 kHz and digitized at 20 kHz. Holding potentials of PCs and INs were -70 mV. The pipette access resistance was compensated by 80%.

During baseline recording for at least 1 min, PFs and CFs were stimulated at 0.2 Hz, whereas putative IN axons were stimulated at 0.33 Hz. To induce DSE at PF-PC and

PF-IN synapses, a depolarizing pulse from -70mV to 0 mV for 5 s was applied to the postsynaptic neurons under recording. To induce DSE at CF-PC synapses, a series of depolarizing pulses (5 depolarizing pulses from -70mV to 0 mV with 100 ms duration repeated at 1 Hz) was applied to PCs. DSE was estimated as the percentage of the first EPSC amplitude after the depolarization relative to the baseline EPSC amplitude for 60 s before the depolarization. To induce DSI at IN-PC synapses, a series of depolarizing pulses (10 pulses of 100 ms duration, from -70 mV to 0 mV, repeated at 1 Hz) was applied to PCs. DSI was estimated as the percentage of the mean amplitude of five consecutive IPSCs after the depolarizing pulse train relative to the baseline IPSC amplitude for 60 s before the train. DHPG (50 μM) was bath-applied for 300 s to examine retrograde suppression by basal RER. DHPG-induced suppression of PF-EPSCs was estimated as the percentage of the mean amplitude of the 3 consecutive PF-EPSCs 170 s after the onset of DHPG application relative to the baseline for 120 s before the agonist application. To induce synaptically-driven mGluR1-mediated retrograde suppression, PFs were repetitively stimulated for 1 s at 50 Hz.

Paired recordings from cultured hippocampal neurons

Cultured hippocampal neurons were prepared from newborn mice as described

previously (9). Each neuron of a pair was whole-cell voltage clamped at –80 mV using a patch pipette (3-5 MΩ) filled with the internal solution containing (in mM) 130 K-gluconate, 15 KCl, 10 HEPES, 0.2 EGTA, 6 $MgCl_2$, 5 Na_2ATP and 0.2 Na_2GTP (pH 7.3, adjusted with KOH). The presynaptic neuron was stimulated by applying positive voltage pulses (to 0 mV, 2 ms) at 0.5 Hz, and IPSCs or EPSCs were recorded from the postsynaptic neuron (9). The external solution for recording IPSCs contained (in mM) 140 NaCl, 2.5 KCl, 2 $CaCl_2$, 1 $MgCl_2$, 10 HEPES, 10 glucose and 1 kynurenic acid (pH 7.3, adjusted with NaOH). For recording EPSCs, the concentration of kynurenic acid was decreased to 0.5 mM. The purpose of the inclusion of 0.5 mM kynurenic acid was to suppress intense spontaneous firings of cultured hippocampal neurons, which is seen when neurons were recorded without partial blockade of excitatory transmission and disturb stable recordings of evoked EPSCs (41).

DSI and DSE were induced by postsynaptic depolarization from –80 mV to 0 mV for 5 s. Magnitudes of DSI and DSE were measured as the percentage of the mean amplitude of IPSCs and EPSCs, respectively, acquired between 4 and 14 s after the end of depolarization relative to that acquired for 30 s before the depolarization. Magnitudes of suppression caused by oxo-M or DHPG were calculated as the percentage of the

mean amplitude of 10 consecutive IPSCs during agonist application relative to the baseline before drug application. All experiments on cultured hippocampal neurons were performed at room temperature.

Recordings from hippocampal slices

Transverse hippocampal slices (300 μm) were prepared from mice aged 19 to 42 postnatally as described previously (42, 43). After cutting, the slices were immediately placed into a reservoir chamber filled with the standard external solution composed of (in mM) 125 NaCl, 2.5 KCl, 2 $CaCl_2$, 1 $MgSO_4$, 1.25 NaH_2PO_4, 26 $NaHCO_3$, and 20 glucose, bubbled with 95% O_2 and 5% CO_2 (pH 7.4), incubated at 36 ºC for ~ 45 min, and then maintained at room temperature.

For recording, a single slice was transferred to a submerged recording chamber. The slice was perfused with an external solution at 32 ºC that contained 2.5 $CaCl_2$ and 1.3 $MgSO_4$ (in mM) and was supplemented with 10 μM NBQX and 5 μM (*R*)-3-(2-carboxypiperazin-4-yl)-propyl-1-phosphonic ((R)-CPP). Whole-cell recordings were made from somata of CA1 pyramidal cells using the same upright microscope with an IR-CCD camera system that was used for recording PCs. Resistance of the patch pipette was 3-5 MΩ when filled with the same cesium-based intracellular solution used

for the DSI experiments in PCs. The pipette access resistance was compensated by 80% and the holding potential was -70 mV. To evoke IPSCs, two patch pipettes filled with the external solution were placed in the stratum radiatum with a tip separation of about 50 ~ 100 μm and this pair was used as a bipolar stimulation electrode. IPSCs were evoked at 0.2 Hz for at least 1 min, and DSI was induced by a series of depolarizing pulses (10 pulses of 100 ms duration, from -70 mV to 0 mV, repeated at 1 Hz). DSI was estimated as the percentage of the mean of the three consecutive IPSC amplitudes after the depolarizing pulse train relative to the baseline for 60 s before the train. For inducing long-term depression of IPSCs (I-LTD), DHPG (100 μM) was bath-applied after stable baseline recordings of IPSCs at 0.2 Hz for at least 20 min. The magnitude of I-LTD was estimated as the percentage of the mean of the IPSC amplitudes 35-40 min after the onset of DHPG application relative to the baseline IPSC amplitude for 5 min just before the DHPG application.

Recordings from striatal slices

For the experiments of the striatum, coronal brain slices containing the cortex and dorsal striatum (300 μm) were prepared from mice at P16-P26 (28).

Whole-cell recordings were made from medium spiny neurons at 32 ºC, using the

same upright microscope with an IR-CCD camera system. Resistance of the patch pipette was 3-5 MΩ when filled with the same cesium-based intracellular solution used for the DSI experiments in PCs and CA1 pyramidal cells. The pipette access resistance was compensated by 80% and the holding potential was -70 mV. The bath solution was supplemented with 10 μM NBQX and 5 μM (R)-CPP.

During baseline recording for at least 1 min, inhibitory inputs to medium spiny neurons were stimulated at 0.2 Hz. To induce DSI, a depolarizing pulse from -70mV to 0 mV (5 s duration) was applied (28). DSI was estimated as the percentage of the mean of the three consecutive IPSC amplitudes after the depolarization relative to the baseline IPSC amplitude for 60 s before the depolarization (28).

Ca^{2+} imaging

For measuring intracellular Ca^{2+}, PCs were loaded for at least 30 min through the patch pipette with the Ca^{2+} indicator Magnesium Green (500 μM) dissolved in the intracellular solution which was composed of (in mM): 110 D-gluconate, 6 KCl, 10 HEPES, 0.2 EGTA, 1 $MgCl_2$, 20 TEA, 2 QX314-Cl, 4 Na-ATP and 0.4 Na-GTP (pH 7.3, adjusted with CsOH). Fluorescence images were acquired by using a high-speed confocal laser-scanning microscope (Yokogawa CSU22, Tokyo, Japan). The Ca^{2+}-dependent

fluorescence signals from distal dendritic regions (Figure 7A) were background-corrected and expressed as the ratio of the stimulus-induced increase in fluorescence over the prestimulus fluorescence value ($\Delta F/F$) using Igor Pro software (Wavemetrics, Lake Oswego, OR).

Immunohistochemistry

For immunohistochemistry, the following affinity-purified primary antibodies were used: anti-mouse DGLα (raised in rabbit) (44), anti-mouse mGluR1α (rabbit) (45), anti-mouse mGluR5 (rabbit) (36), anti-mouse PLCβ1 (guinea pig) (46), anti-mouse PLCβ4 (guinea pig) (47), anti-mouse CB_1 (guinea pig) (22) antibodies, and anti-mAChR-M1 (rabbit) (28). Brain sections were incubated with 10% normal donkey serum for 20 min, primary antibodies overnight (All primary antibodies were used at the final concentration of 1 μg/ml), and indocarbocyanine (Cy3)-labeled species-specific secondary antibodies for 2 h at a dilution of 1:200 (Jackson ImmunoResearch, West Grove, PA). Phosphate-buffer saline containing 0.1% Tween 20 was used as a diluent buffer for NeuroTrace and antibodies and as a washing buffer. Images were taken with a fluorescence microscope (AX-70; Olympus, Tokyo, Japan) equipped with a digital camera (DP70; Olympus) or with a confocal laser scanning microscope (FV1000;

Olympus).

Western blot analysis

Adult cerebellum, hippocampus and striatum from wild type, α-KO, and β-KO mouse were homogenized in homogenate buffer (0.32 M sucrose, 5 mM EDTA, 10 mM Tris-Cl [pH 7.2] and protease inhibitor cocktail [Roche Applied Sciences. Meylan, France]), and then centrifuged at 1000 × g for 10 min. Total protein concentration of the supernatant was measured using BCA Protein Assay Kit (Pierce, Rockford, IL). Protein samples were separated by sodium dodecylsulfate (SDS)-polyacrylamide gel electrophoresis (PAGE), and immunoreaction was performed using the same primary antibodies described in the immunohistochemistry section.

Quantification of 2-AG and anandamide

For measuring basal contents of 2-AG and anandamide in the cerebellum, striatum and hippocampus, block samples were obtained from mice at 2-6 months of age, frozen immediately in liquid nitrogen, and stored at -80 ºC. For measuring stimulus-induced production of 2-AG and anandamide, eight parasagittal cerebellar slices (250 μm) were cut from each of the mutant and wild-type mice at P15-P30 in an external solution with the following composition (in mM): 120 choline-Cl, 2 KCl, 28 $NaHCO_3$, 1.25 NaH_2PO_4,

8 $MgCl_2$, and 20 glucose (bubbled with 95% O_2 and 5% CO_2). Slices were incubated for 5h in the same choline-based external solution at room temperature, and then transferred to a chamber filled with the normal external solution containing 1 μM tetrodotoxin to prevent synaptic transmission for 10-15 min. Slices were perfused with the normal external solution containing 1 μM tetrodotoxin, 100 μM DHPG and 20 mM KCl for 1 min to evoke endocannbinoid production. Then, samples were frozen immediately in liquid nitrogen, and stored at -80 ºC.

The samples were crushed to powder without thawing using AutoMill (Tokken, Chiba, Japan) and lipids were extracted with 1 ml of acetonitrile containing deuterized 2-AG (2-AG-d8, Cayman, Ann Arbor, MI) as an internal standard. The extracts were further cleaned up and concentrated using Oasis HLB solid phase extraction cartridge (Waters, Milford, MA). Samples were diluted 3-fold with water containing 0.03% formic acid and loaded to preconditioned Oasis HLB cartridge. The cartridges were serially washed with water and 15% ethanol, and then eluted with 150 μl of acetonitrile, 5 μl of which were analyzed with a liquid chromatography-tandem mass spectrometry (LC-MS/MS) system.

An ultra-performance liquid chromatography (UPLC, Waters) and a TSQ Quantum

Ultra triple-stage quadrupole mass spectrometer (Thermo Scientific, Waltham, MA) were used. The following UPLC conditions were used: column, ACQUITY UPLC BEH C18 (1.0 mm x 100 mm); flow rate, 100 μl/min; mobile phase, A: 20 mM NH_4HCO_3, B: acetonitrile; gradient program, 20-95% of mobile phase B (0-20min) and hold at 95% of B (20-27 min); column temperature, 45 ºC. With this condition, 2-AG was baseline resolved from its structural isomer 1-AG. TSQ Quantum Ultra mass spectrometer with electrospray ionization ion source was operated in selected-reaction monitoring (SRM) mode under the following conditions: spray voltage, +3.5 kV, ion transfer tube temperature, 350C; sheath gas, 65; aux gas, 5; collision gas, 1.2 mTorr; Q1 and Q3 resolution, both at 0.7; SRM transitions, *m/z* 379 →287 (2-AG), *m/z* 387 → 294 (2-AG-d8) and *m/z* 384 → 62 (anandamide). Quantification was performed with internal standard method using 2-AG-d8 as an internal standard for both 2-AG and anandamide. Data were analyzed with Xcalibur 2.0.6 software package (Thremo Scientific).

Results

Generation of DGLα and DGLβ knockout mice

I generated null mutant mice lacking either DGLα or DGLβ by homologous recombination using the ES cell line RENKA, which I developed from the C57BL/6N strain (38), followed by Cre-mediated deletion of the targeted genes (Figure 4, Experimental Procedures). DGLα knockout (α-KO) and DGLβ knockout (β-KO) mice were generated by disrupting exon 3 and 4 of *Dagla* gene (Figures 4A and 4C) and exon 10 and 11 of *Daglb* gene (Figures 4B and 4E), respectively. The resulting α-KO and β-KO mice are viable and appear normal with regard to their general appearances. Nissl staining of brains of α-KO and β-KO mice show that there are no perceptive abnormalities in the two knockout mice (Figure 5A). I verified that DGLα expression was normal in the brain of β-KO mice (Figure 5B), whereas DGLα immunoreactivity was totally absent in α-KO mice (Figures 4D and 5B). I confirmed that the DGLβ transcript was absent in the forebrain and cerebellum of β-KO mice (Figure 4F). I examined basic properties of synaptic transmission in acute slices of the cerebellum and striatum. Overall, kinetics of synaptic currents and paired-pulse ratio of α-KO and β-KO mice were not different from their wild-type (WT) littermates (Table 1). I

measured basal 2-AG contents in the cerebellum, striatum and hippocampus, and found that the 2-AG contents were markedly decreased in α-KO mice (Figure 4G), whereas they were normal in the three brain regions of β-KO mice (Figure 4G). Therefore, contribution of DGLα to 2-AG biosynthesis seems to be much greater than DGLβ in the CNS. In addition, basal contents of AEA were decreased in the cerebellum and hippocampus of α-KO mice, whereas they were normal in β-KO mice (Figure 5C).

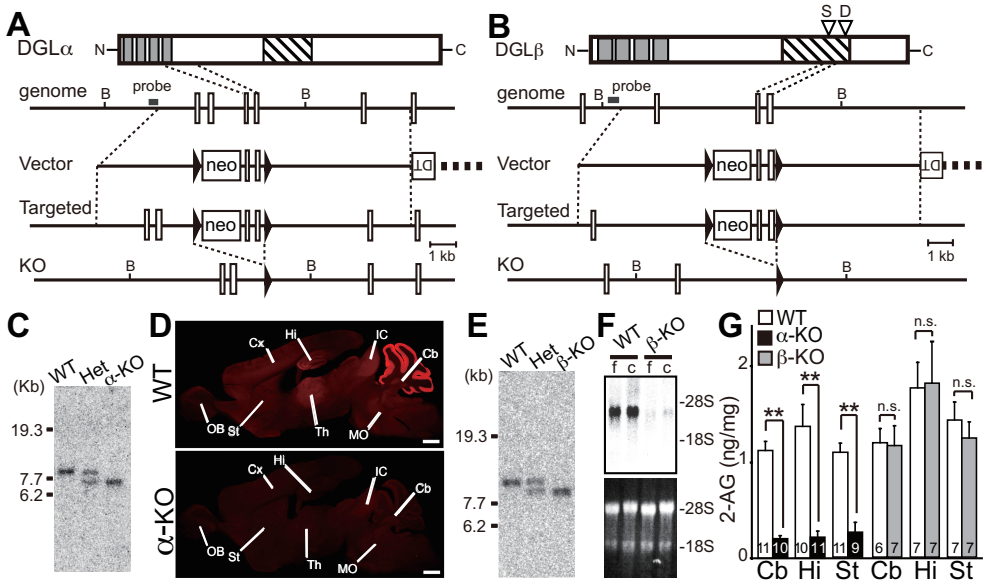

Figure 4. Generation of DGLα knockout (α-KO) and DGLβ knockout (β-KO) mice. (**A, B**) Knockout strategy of *Dagla* (**A**) and *Daglb* (**B**) *genes*. Homologous recombination of the targeting plasmid resulted in insertion of the pgk-neo cassette (neo) and *loxP* sequences (filled triangles) into intron 2 and 4 of *Dagla* gene (**A**) or intron 9 and 11 of *Daglb* gene (**B**). After homologous recombination in ES cells followed by germline transmission (*Targeted*) the floxed mice were crossed with "Cre-deleter" mice. Exon 3 and 4 of *Dagla* gene (**A**) or exon 10 and 11 of *Daglb* gene (**B**) were deleted from germline (*KO*) together with the neo cassette. Four putative transmembrane domains and the serine lipase motif are indicated with grey and striped boxes, respectively. In **(B)**, two putative catalytic triad serine and aspartate are indicated with inverted open triangles. B, *Bgl* II. (**C**) After Cre-mediated excision of exon 3 and 4 of *Dagla* gene, the *Bgl* II-digested 7.9 kb (WT) band shifted to 7kb (α-KO). (**D**) Lack of DGLα immunofluorescence in α-KO brain. In WT mice, DGLα is expressed strongly in the cerebellar cortex and moderately in other brain regions including the hippocampus and striatum. (**E**) After Cre-mediated excision of exon 10 and 11 of *Daglb* gene, the *Bgl* II-digested 8.9 kb (WT) band shifted to 7.95 kb (β-KO). (**F**) Lack of DGLβ transcript in β-KO mice. Northern blot analysis of total RNA samples from the forebrain **(f)** and cerebellum **(c)** of WT and β-KO mice (upper panel) and ethidium bromide staining of the corresponding agarose gel showing 28S and 18S ribosomal RNAs (lower panel). (**G**) Amount of 2-AG in block samples of cerebellum, striatum and hippocampus from WT, α-KO and β-KO mice. The number of samples is indicated within each column. **$p < 0.01$ See also Figure 5 and Table 1.

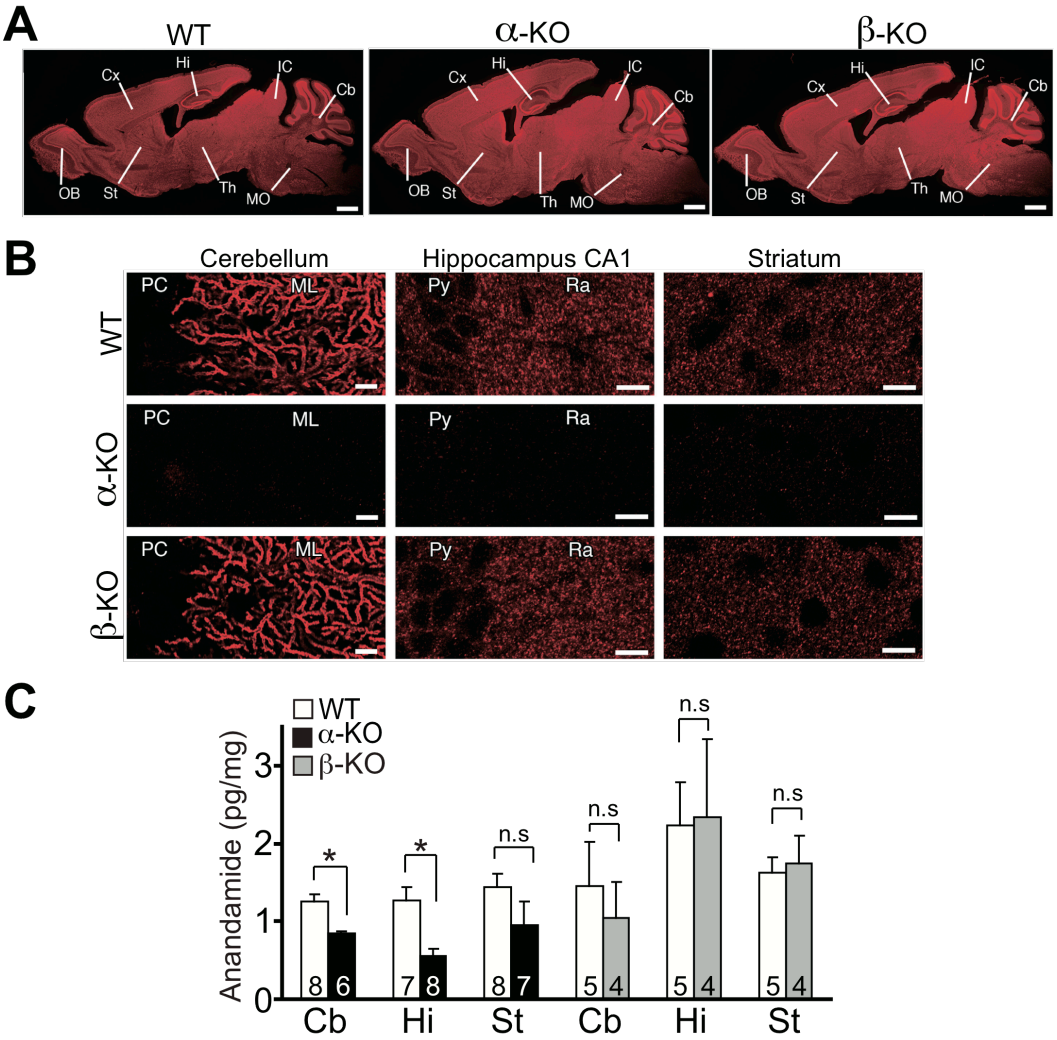

Figure 5. Brain histology and Amount of Anandamide of α-KO and β-KO mice. (**A**) Normal brain histology of α-KO and β-KO mice. Nissl staining of parasagittal brain sections. Cb, cerebellum; Cx, cerebral cortex; Hi, Hippocampus; IC, inferior colliculuc; MO, medulla oblongata; OB, olfactory bulb; St, striatum; Th, thalamus. Scale bars, 1mm. (**B**) High-power magnification images of immunofluorescence for DGLα in the cerebellum (left), hippocampal CA1 region (middle), and striatum (right). A tubular pattern of dendritic surface staining in cerebellar PCs, and a punctate pattern in the neuropil of the hippocampal CA1 region and striatum are depicted in WT and β-KO mice, while these characteristic expression patterns are totally absent in α-KO mice. ML, molecular layer; PC, Purkinje cell layer; Py, pyramidal cell layer; Ra, stratum radiatum. Scale bars, 10 mm. (**C**) Amount of anandamide in block samples of cerebellum, striatum and hippocampus from WT, α-KO and β-KO mice. The number of samples is indicated within each column. *$p < 0.05$

	Brain region		WT	α-KO	β-KO
10 – 90 % Rise Time (ms)	Cerebellum	CF-EPSC	0.63±0.05 (n = 24)	0.66±0.15 (n = 13)	0.56±0.03 (n = 6)
		PF-EPSC	1.03±0.07 (n = 33)	1.00±0.07 (n = 12)	1.05±0.08 (n = 15)
		IPSC	0.72±0.05 (n = 21)	0.76±0.08 (n = 15)	0.87±0.10 (n = 5)
	Striatum	IPSC	0.77±0.07 (n = 22)	0.77±0.04 (n = 31)	ND
Decay Time Constant (ms)	Cerebellum	CF-EPSC	3.72±0.30 (n = 24)	3.18±0.43 (n = 13)	3.47±0.34 (n = 6)
		PF-EPSC	5.86±0.40 (n = 33)	5.28±0.46 (n = 15)	5.07±0.59 (n = 12)
		IPSC	4.43±0.32 (n = 21)	5.14±0.48 (n = 15)	4.36±0.32 (n = 7)
	Striatum	IPSC	6.17±0.31 (n = 22)	6.79±0.26 (n = 31)	ND
Paired – Pulse Ratio (2_{nd} / 1_{st})	Cerebellum	CF-EPSC	0.41±0.04 (n = 24)	0.38±0.04 (n = 17)	0.47±0.06 (n = 6)
		PF-EPSC	1.58±0.02 (n = 28)	1.56±0.05 (n = 19)	1.49±0.03 (n = 9)
		IPSC	0.86±0.03 (n = 20)	0.78±0.04 (n = 14)	0.83±0.04 (n = 8)
	Striatum	IPSC	0.75±0.04 (n = 21)	0.77±0.03 (n = 19)	ND
		(mean ± SE)			

ND, Not determined

Table 1. Rise time, decay time constant and paired-pulse ratio of synaptic currents in WT, α-KO and β-KO.

Retrograde suppression is deficient in the DGLα knockout cerebellum

I examined retrograde suppression of synaptic transmission by the three modes of endocannabinoid release in acute cerebellar slices. In WT mice, strong depolarization of PCs caused Ca^{2+}-driven ER and readily induced transient suppression of excitatory synaptic transmission (DSE) from PFs (Figures 6A and 6B “PF-PC”) and CFs (Figure 6B “CF-PC”) as well as of synaptic transmission from inhibitory interneurons (INs) (DSI) (Figure 6B “IN-PC”). DSE also occurred at PF to IN synapses following depolarization of INs (Figure 6B “PF-IN”). By marked contrast, DSE and DSI were totally absent in PCs and INs of α-KO mice (Figures 6A and 6B). I verified that Ca^{2+} transients in PCs following DSE/DSI-inducing depolarization (Figures 7A - 7D) and cannabinoid sensitivities of PFs, CFs and inhibitory synaptic terminals (Figure 7E) were normal in α-KO mice. These results indicate that the deficiency of DSE/DSI in α-KO

cerebellum is not attributable to decreased Ca^{2+} transients, and that DGLα is indispensable for Ca^{2+}-driven ER in the cerebellum.

I then examined whether basal RER and Ca^{2+}-assisted RER were affected by deletion of DGLα. To test basal RER, I activated metabotropic glutamate receptor–subtype 1 (mGluR1), a $G_{q/11}$-coupled receptor strongly expressed in PCs, by bath application of its agonist, *R,S*-3,5-dihydroxyphenylglycine (DHPG). DHPG (50 μM) readily induced reversible suppression in WT mice but this receptor-mediated suppression was totally absent in α-KO mice (Figure 6C). As for Ca^{2+}-assisted RER, marginal DSE at CF-PC synapse by weak depolarization of PCs was prominently enhanced when combined with subthreshold mGluR1 activation by a low dose of DHPG (10 μM) in WT mice (27) (Figures 6D and 6E). Furthermore a brief burst of PF stimulation caused Ca^{2+}-assisted RER by synaptically activated mGluR1 and transiently suppressed PF-PC transmission in WT mice (27, 48) (Figure 6F), which was reversed to a transient potentiation by the CB_1 antagonist AM251. Notably, both forms of Ca^{2+}-assisted RER were totally absent in α-KO mice (Figures 6D, 6E and 6F). I verified that expression patterns and protein levels of molecules involved in endocannabinid signaling (mGluR1, PLCβ4, and CB_1) (21, 27, 44) and

mGluR1-mediated slow EPSCs in PCs (49) were normal in the α-KO cerebellum (Figure 8A-C). These results indicate that the lack of basal and Ca^{2+}-assisted RER in the cerebellum of α-KO mice is not attributable to changes in the expression of endocannabinoid signaling molecules. I also performed a biochemical experiment to measure stimulus-induced production of 2-AG in cerebellar slices. Combined application of DHPG (100 μM) and high K^+ (20 mM) solution elevated 2-AG level in WT mice (Figure 6G), which mimicked Ca^{2+}-driven RER in electrophysiological experiments (27). In contrast, this combined stimulation caused no elevation of 2-AG in α-KO mice (Figure 6G). Importantly, the same stimulation caused no change in AEA contents in cerebellar slices of WT and α-KO mice (Figure 6H). These results indicate that DGLα is indispensable for basal and Ca^{2+}-assisted RER in the cerebellum.

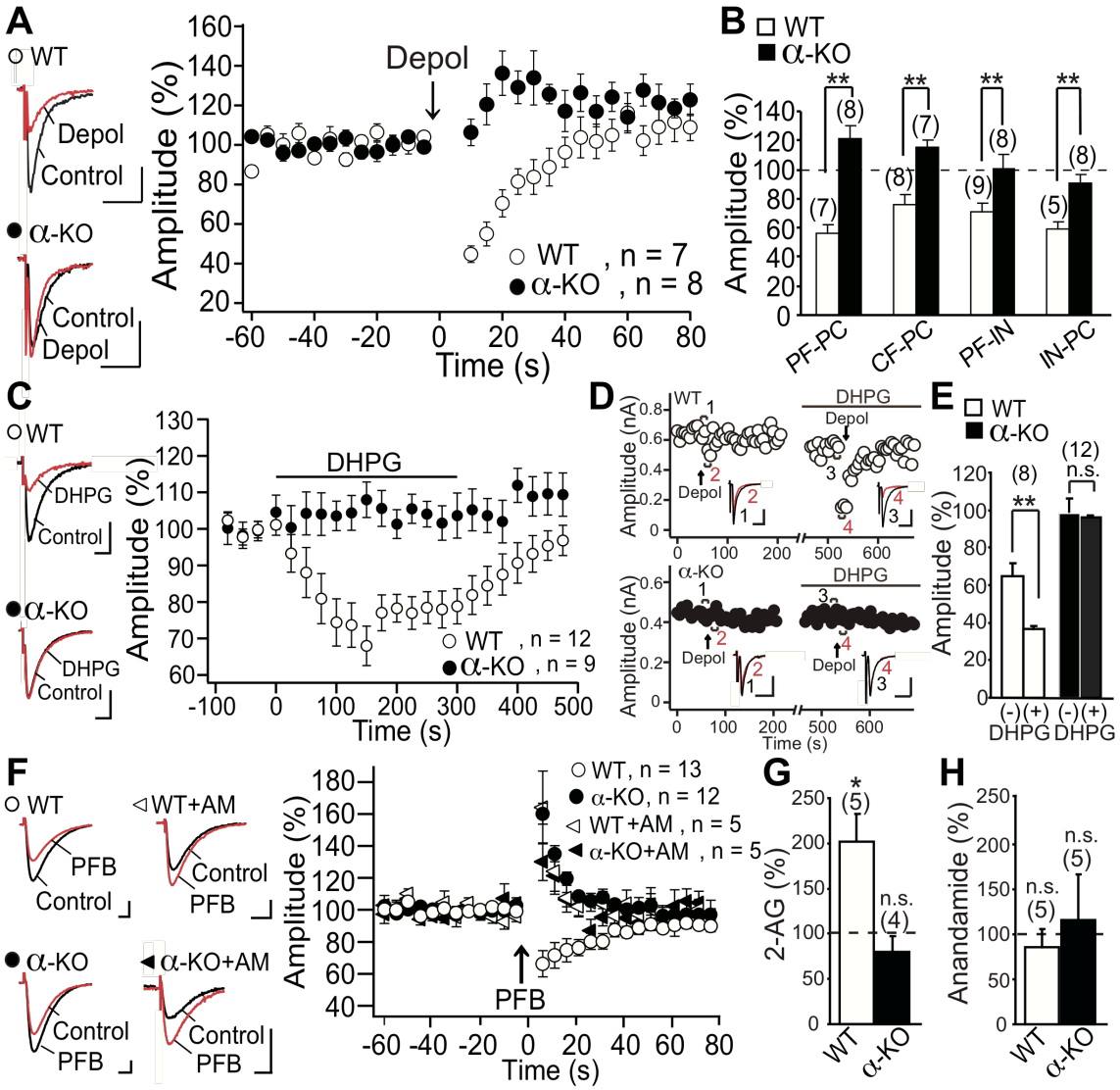
A
WT
Depol
Control
α-KO
Control
Depol
Depol
Amplitude (%)
Time (s)
WT , n = 7
α-KO , n = 8
B
WT
α-KO
Amplitude (%)
PF-PC
CF-PC
PF-IN
IN-PC
C
WT
DHPG
Control
α-KO
DHPG
Control
DHPG
Amplitude (%)
Time (s)
WT , n = 12
α-KO , n = 9
D
WT
DHPG
Depol
α-KO
Amplitude (nA)
Time (s)
E
WT
α-KO
Amplitude (%)
DHPG
F
WT
WT+AM
PFB
Control
Control
PFB
α-KO
α-KO+AM
Control
PFB
Control
PFB
Amplitude (%)
PFB
Time (s)
WT, n = 13
α-KO, n = 12
WT +AM , n = 5
α-KO+AM , n = 5
G
2-AG (%)
n.s.
WT
α-KO
H
Anandamide (%)
n.s.
n.s.
WT
α-KO

Figure 6. Endocannabinoid-mediated retrograde suppression is absent in the cerebellum of α-KO mice. **(A)** Sample traces (left) and average time courses of PF-mediated EPSCs (right) from PCs of WT and α-KO mice before and after depolarization of PCs. **(B)** Summary bar graph showing the magnitudes of DSE at PF-PC, CF-PC, and PF-IN synapses, and those of DSI at IN-PC synapse. DSE at PF-PC and PF-IN synapses were induced by depolarizing postsynaptic neurons from -70mV to 0 mV for 5 s. DSE at CF-PC synapses and DSI at IN-PC synapses were induced by a series of depolarizing pulses to PCs (5 [for DSE] and 10 [for DSI] depolarizing pulses from -70mV to 0 mV with 100 ms duration at 1 Hz). **(C)** Sample traces (left) and average time courses of PF-EPSCs (right) before, during and after bath application of DHPG (50 μM). **(D** and **E)** Representative experiment **(D)** and summary bar graph **(E)** showing enhancement of marginal DSE of CF-mediated EPSCs by weak depolarization (from -70 mV to 0 mV for 0.1 s) in the presence of a low dose (10 μM) of DHPG. **(F)** Sample traces (left) and average time courses of PF-EPSCs (right) before and after a burst of PF stimulation (PFB, 50 Hz, 50 pulses) recorded from PCs of WT mice and α-KO mice in the normal external solution or after treatment of AM251 (5 μM). **(G** and **H)** Summary bar graphs showing the percent changes in the 2-AG **(G)** and anandamide **(H)** levels of cerebellar slices from WT and α-KO mice after combined DHPG (100 μM) and high K^+ (20 mM) stimulation for 1min.

The number of cells for each experiment is indicated in parenthesis (**B**, **E , G** and **H**). Calibration bars: 0.1 nA and 5 ms for **(A)**, **(C)** and **(F)**, and 0.2 nA and 5 ms for (**D**). $*P < 0.05$, $**P < 0.01$. See also Figure 7 and 8.

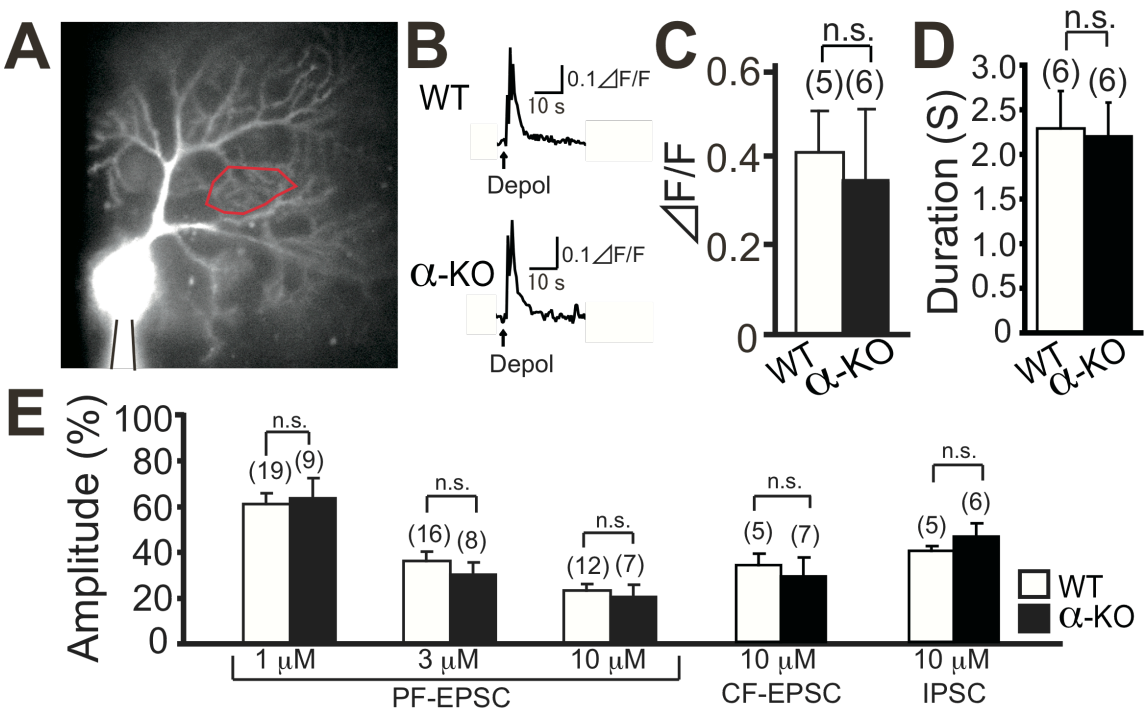

Figure 7. Depolarization-induced Ca^{2+} transients in PCs and cannabinoid sensitivities of synapses in the cerebellum are normal in α-KO mice. (**A**) Representative fluorescent image of a PC from WT mouse showing a distal dendritic region (demarcated with red line) from which Ca^{2+} transients were measured. (**B-D**) Representative traces (**B**) and summary bar graphs for the amplitude (**C**) and the duration (half width) (**D**) of Ca^{2+} transients elicited by a series of depolarizing pulses (3 pulses of 100 ms duration from -70 mV to 0 mV, repeated 1 Hz). The duration (half width) was measured as the time between the data points of Ca^{2+} transient crossing the half maximum amplitudes. Arrows in (**B**) indicate the onsets of depolarization. There were no significant differences in the amplitudes and the duration of Ca^{2+} transients between WT and α-KO PCs ($p > 0.05$). (**E**) Summary bar graphs showing the magnitudes of presynaptic suppression indced by the CB_1 agonist WIN55, 212-2 for PF-EPSC, CF-EPSC and IPSC in the cerebellum. The concentration of WIN55, 212-2 is indicated below each set of columns. There were no significant differences between WT and α-KO mice ($p > 0.05$).

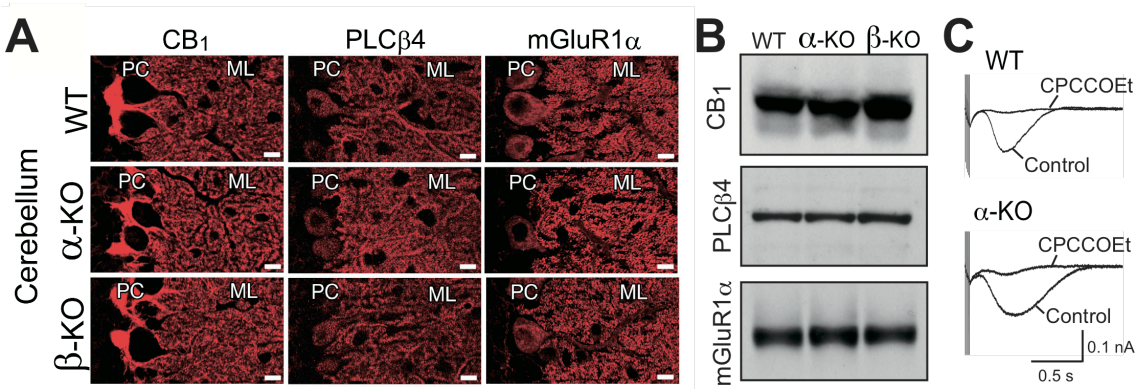

Figure 8. Comparable expression levels and distribution of molecules for 2-AG-mediated retrograde suppression in the cerebellum of WT (upper panels), α-KO (middle panels) and β-KO (bottom panels) mice. (**A**) Immunofluorescence for CB_1, PLCβ4 and mGluR1α in the cerebellum. ML, molecular layer; PC, Purkinje cell layer. Scale bars, 10 mm. (**B**) Western blot analysis of cerebellar homogenate samples (10 μg) shows no obvious change in the expression levels of CB_1, PLCβ4 and mGluR1α in the α-KO and β-KO cerebella. (**C**) Representative traces of slow EPSCs in WT and α-KO PCs induced by a brief burst (100 Hz, 5 pulses) of PF stimulation in the presence of NBQX (10 μM) to block AMPA receptor-mediated fast EPSCs. Traces taken before and after bath application of the mGluR1 antagonist CPCCOEt (100 μM) are superimposed. Amplitudes of mGluR1-mediated slow EPSC were 117.4 ± 17.9 pA for WT mice (n = 7) and 102.9 ± 25.4 pA for α-KO mice (n = 9) with no significant difference ($p > 0.05$).

Retrograde suppression is deficient in the hippocampus and striatum of DGLα knockout mice

I then examined endocannabinoid-mediated retrograde suppression in the hippocampus and striatum. In cultured hippocampal neurons, paired whole-cell recordings were performed and EPSCs and cannabinoid-sensitive unitary IPSCs were pharmacologically isolated. In WT mice, DSI (Figures 9A and 9B) and DSE (Figure 9B) were readily induced in the cannabinoid-sensitive IPSCs and EPSCs, respectively, following depolarization of the postsynaptic neuron from -80 mV to 0 mV for 5 s(9, 42). The same depolarization protocols caused no appreciable suppression in IPSCs or EPSCs in hippocampal cultures prepared from α-KO mice (Figures 9A and 9B). In WT hippocampal neurons, activation of $G_{q/11}$-coupled receptors, mGluR5 by DHPG and M_1/M_3 muscarinic acetylcholine receptors (mAChR-M_1/M_3) by oxotremorine-M (oxo-M), readily induced endocannabinoid-mediated retrograde suppression of IPSCs (Figure 9B). By contrast, these forms of receptor-mediated retrograde suppression were totally absent in α-KO mice (Figure 9B).

I also examined endocannabinoid-mediated retrograde suppression in hippocampal slices. Whole-cell recordings were made from CA1 pyramidal cells and IPSCs were

evoked by stimulation in the stratum radiatum. DSI was readily induced by a series of depolarizing pulses (10 pulses of 100 ms duration, from -70 mV to 0 mV, repeated at 1 Hz) in WT mice, whereas DSI was totally absent in α-KO mice (Figure 9B). Bath application of DHPG (100 μM) caused long-term depression of IPSCs (I-LTD) in WT mice, as reported previously (34). In contrast, DHPG failed to induce I-LTD in α-KO mice (Figure 10A).

In striatal slices, whole-cell recordings were performed from medium spiny neurons and inhibitory inputs were stimulated around the recorded neurons (28, 50). In WT mice, DSI was readily elicited by a depolarizing pulse from -70mV to 0 mV (5 s duration) (Figure 9B), and marginal DSI by a short-depolarization (a depolarizing pulse from -70mV to 0 mV, 1 s duration) was significantly enhanced by a low dose (0.5 μM) of oxo-M (Figures 9C and 9D). By marked contrast, DSI (Figure 9B) and the enhancement of marginal DSI by a low dose of oxo-M (Figures 9C and 9D) were totally absent in α-KO mice.

I verified that cannabinoid sensitivities of IPSCs in hippocampal and striatal slices were normal in α-KO mice (Figure 10B). Furthermore, I confirmed expression patterns and protein levels of molecules required for endocannabinid signaling in the

hippocampus and striatum (26, 36, 44) including mGluR5, mAChR-M_1, PLCβ1 and CB_1 were normal in α-KO mice (Figure 11). Thus, the lack of endocannabinoid-mediated retrograde suppression in their hippocampus and striatum must result from the lack of DGLα.

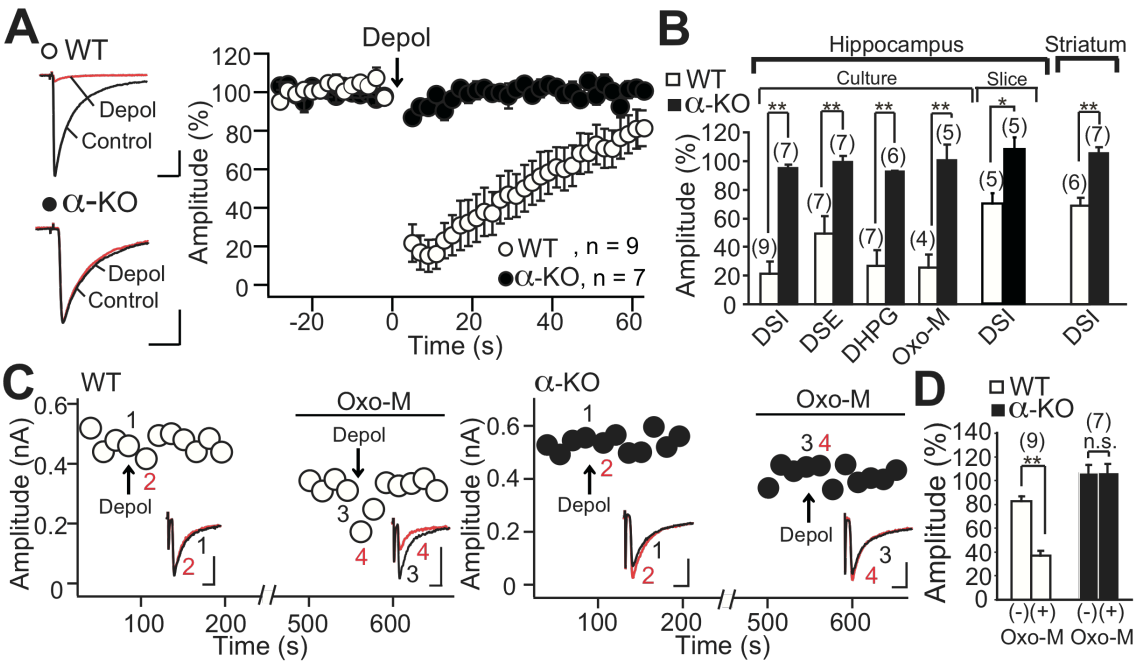

Figure 9. Endocannabinoid-mediated retrograde suppression is absent in the hippocampus and striatum of α-KO mice. **(A)** Sample traces (left) and average time courses of DSI (right) in cultured hippocampal neurons of WT and α-KO mice before and after depolarization (from -80 mV to 0 mV, for 5 s). **(B)** Summary bar graph showing the magnitudes of DSI, DSE and retrograde suppression induced by DHPG and oxo-M in cultured hippocampal neurons, and those of DSI in hippocampal and striatal slices. **(C** and **D)** Representative experiments **(C)** and summary bar graph **(D)** showing the enhancement of marginal DSI (induced by depolarization from -70 mV to 0 mV for 0.1 s) by a low dose of oxo-M (0.5 μM) from medium spiny neurons of WT and α-KO striatum.

The number of cells for each experiment is indicated in parenthesis (**B** and **D**). Calibration bars: 0.2 nA and 5 ms for **(A)** and **(C)**. $^{**}P < 0.01$. See also Figures 10 and 11.

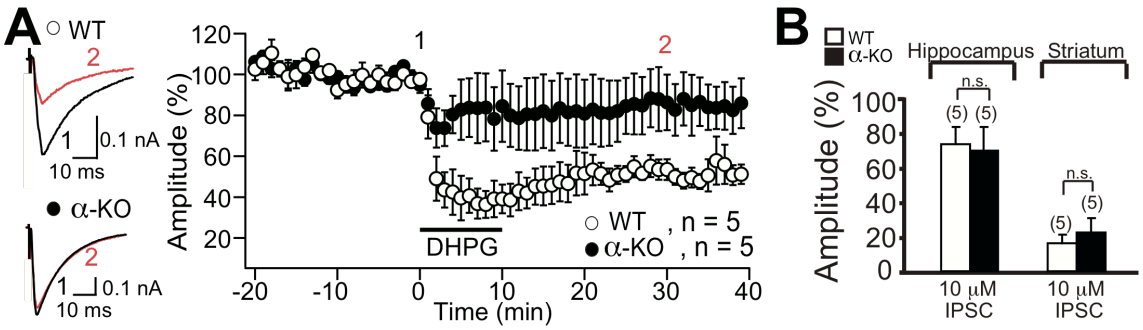

Figure 10. Long-term synaptic plasticity in the hippocampus. CB_1 sensitivity in the hippocampus and the striatum. (**A**) Long-term depression of inhibitory synaptic transmission (I- LTD) is absent in the hippocampus of α-KO mice. Sample traces of IPSC (left) and average time courses of I- LTD (right) in CA1 pyramidal cells of WT and α-KO mice before, during and after bath application of DHPG (100 μM). Traces obtained at the time points 1 and 2 in (right) are superimposed in (left). Clear I- LTD was induced in WT mice (53.3 ± 7.4 %, measured 35 – 40 min after the onset of DHPG application relative to the baseline value for 5 min just before the agonist application. $p < 0.001$), whereas I-LTD was absent in α-KO mice (84.0 ± 14.4 %, $p > 0.05$). (**B**) Summary bar graphs showing the magnitudes of presynaptic suppression induced by the CB_1 agonist WIN55, 212-2 (10 μM) for IPSC in the hippocampus and the striatum. There were no significant differences between WT and α-KO mice ($p > 0.05$).

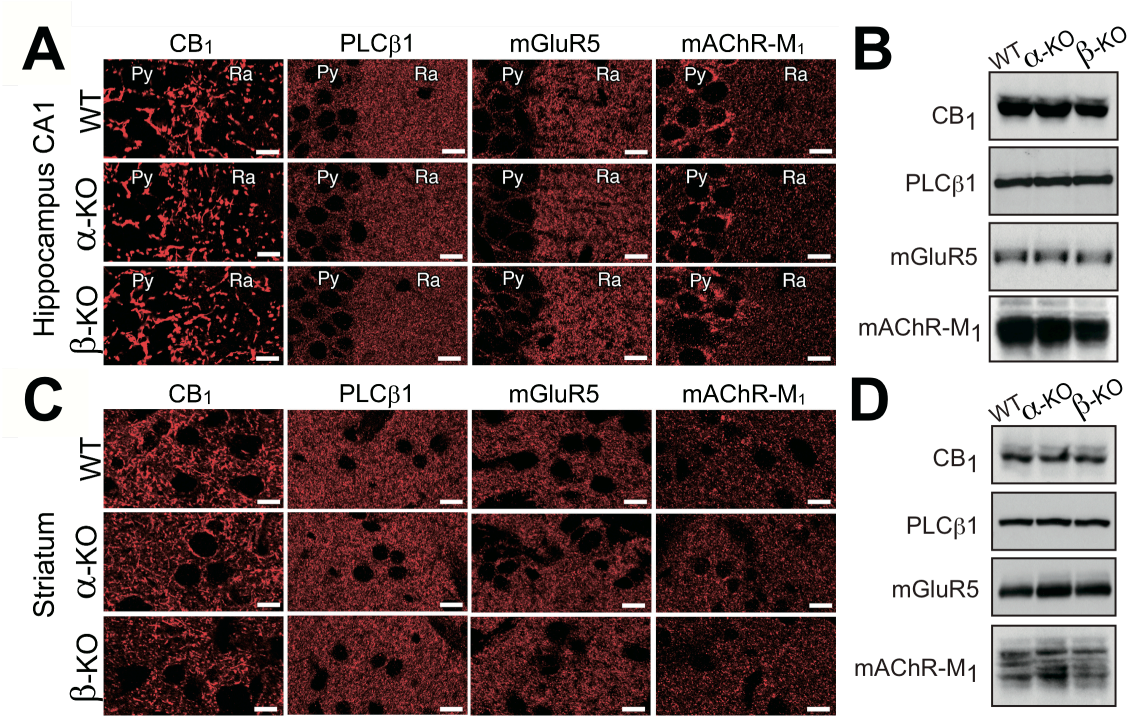

Figure 11. Comparable expression levels and distribution of molecules for 2-AG -mediated retrograde suppression in the hippocampus and striatum of WT (upper panels), α-KO (middle panels) and β-KO (bottom panels) mice. (**A** and **C**) Immunofluorescence for CB1, PLCβ1, mGluR5 and mAChR-M_1 in the hippocampus CA1 region (**A**) and in the striatum (**C**). Scale bars, 10 mm. (**B** and **D**) Western blot analysis of homogenate samples from the hippocampus (10 μg) (**B**) and striatum (20 μg) (**D**) show no obvious change in the expression levels of CB_1, PLCβ1, mGluR5 and mAChR-M_1 in the α-KO and β-KO mice.

Retrograde suppression is normal in DGLβ knockout mice

I then examined whether DGLβ also contributes to retrograde signaling. Morphology of the brain (Figure 5A) and expression patterns and protein levels of mGluR1/5, PLCβ1/4, mAChR-M_1, DGLα and CB_1 were normal in β-KO mice (Figures 8 and 11). I used the same experimental protocols to induce Ca^{2+}-driven ER, basal RER or Ca^{2+}-assisted RER as used for WT and α-KO mice. I found that DSE at PF-PC synapses (Figures 12A and 12B) and DSI at IN-PC synapses (Figure 12B) in the cerebellum and DSI in cultured hippocampal neurons (Figures 12D and 12E) were normal in β-KO mice. Suppression of IPSCs induced by DHPG or oxo-M in hippocampal neurons was also normal (Figure 12E). Furthermore, suppression of PF-PC transmission by a PF burst was normal in β-KO mice (Figure 12C). Therefore, the three modes of endocannabinoid release, Ca^{2+}-driven ER, basal RER or Ca^{2+}-assisted RER, are intact in β-KO mice.

Taken together, the present results strongly suggest that 2-AG produced by DGLα, not by DGLβ, mediates retrograde signaling at central synapses.

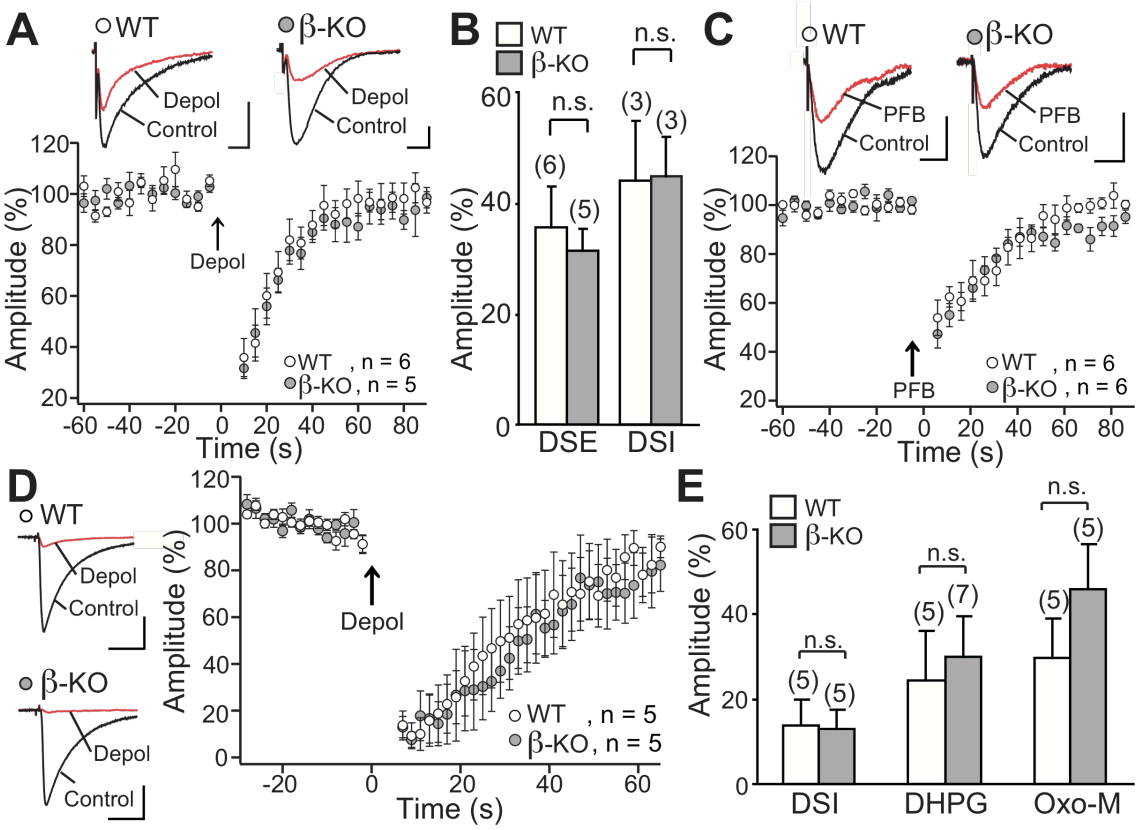

Figure 12. Endocannabinoid-mediated retrograde suppression is intact in the cerebellum and hippocampus of β-KO mice.

(A) Sample traces and average time courses of PF-mediated EPSCs from PCs of WT and β-KO mice before and after depolarization of PCs. **(B)** Summary bar graph showing the magnitudes of DSE at PF-PC synapse and DSI at IN-PC synapse in the cerebellum. **(C)** Sample traces and average time courses of PF-EPSCs before and after a burst of PF stimulation (PFB, 50 Hz, 50 pulses) recorded from PCs of WT and β-KO mice. **(D)** Similar to **(A)** but for DSI in cultured hippocampal neurons. **(E)** Similar to **(B)** but for magnitudes of DSI, DHPG-induced suppression, and Oxo-M-induced suppression in the hippocampus.

The number of cells for each experiment is indicated in parenthesis (**B** and **E**). Calibration bars: 0.1 nA and 10 ms for **(A)** and **(C)**, and 0.2 nA and 20 ms for **(D)**.

See also Figures 8 and 11.

Discussion

I found that the three modes of endocannabinoid release and resultant retrograde suppression of synaptic transmission were totally absent in the cerebellum, hippocampus and striatum of α-KO mice. The basal 2-AG content was markedly reduced in the three brain structures and the stimulus-induced elevation of 2-AG levels was absent in the cerebellum of α-KO mice. By contrast, endocannabinoid-mediated synaptic suppression and 2-AG content were normal in β-KO mice. Although the anandamide level was reduced in the cerebellum and hippocampus of α-KO mice, the extent of reduction was much smaller than 2-AG content. The cerebellum, hippocampus and striatum have been most extensively studied for the mechanisms of endocannabinoid-mediated synaptic modulation. Many previous studies suggest that synapses in other brain regions share the same mechanisms of endocannabinoid release as those in the three brain structures (11, 51-54). Therefore, my results suggest that 2-AG produced by DGLα, not by DGLβ, likely accounts for most retrograde signaling at synapses throughout the CNS, although the possibility remains that anandamide or other endocannabinoids may be involved in other synapses.

Previous biochemical studies have revealed several pathways for 2-AG generation

(55-57). In the main pathway, PLCβ activated by $G_{q/11}$ hydrolyzes arachidonic acid-containing membrane phospholipid such as phosphatidylinositol, and produces arachidonic acid-containing diacylglycerol. Then, 2-AG is produced from the diacylglycerol by the action of DGLα and/or DGLβ. Besides this main cascade, alternative pathways for 2-AG generation are proposed, which include the sequential reactions by phospholipase A_1 (PLA_1) and lysoPI-specific PLC, the conversion from 2-arachidonoyl lysophosphatidic acid to 2-AG by phosphatase, and the formation from 2-arachidonoyl phosphatidic acid through 1-acyl-2-arachidonoylglycerol. However, the present results indicate that these alternative pathways are not involved in 2-AG generation for retrograde synaptic suppression.

Previous studies indicate that DGLα is expressed at postsynaptic sites of the neurons in various regions of the CNS (36, 44, 58, 59). DGLα is most abundant around dendritic spines and is apposed closely to $G_{q/11}$-coupled receptors, $G_{q/11}$ protein α subunit, and PLCβ. Such a subcellular arrangement of molecules constitutes an anatomical basis for basal and Ca^{2+}-assisted RER (11, 60). The density of CB_1 expression in excitatory and inhibitory presynaptic terminals and the distances between the presynaptic terminals and the DGLα-rich postsynaptic structures are unique to each brain region (61,

62). DGLα seems to be arranged such that the induction threshold of 2-AG-mediated retrograde suppression of excitation and inhibition may be coordinated. In DGLα knockout mice, basal and Ca^{2+}-assisted RER was totally absent, although subcellular localizations of $G_{q/11}$-coupled receptors, PLCβ and CB_1 were normal. Thus, the primary function of DGLα in central neurons seems to be the production of 2-AG that mediates retrograde synaptic suppression.

In contrast to DGLα, relatively little is known about subcellular localization of DGLβ at synapses. DGLβ was reported to be richly expressed in the PC soma but very low in dendrites (63). This expression pattern is clearly different from DGLα (44). I expected that DSI of IN-PC synapse would have been smaller in β-KO mice if DGLβ in the PC soma had played a role in 2-AG production, since in this experiment I stimulated putative BC axons that form inhibitory synapses on the PC soma. However, my results demonstrate that DSI is normal in β-KO mice, suggesting that DGLβ has no contribution to retrograde synaptic suppression in PCs. In a recent study, DGLβ and DGLα were reported to be co-expressed in postsynaptic sites facing CB_1 rich excitatory terminals in the dorsal cochlear nucleus (64). It is possible that DGLβ may participate in 2-AG production at synapses in limited brain regions.

Besides retrograde suppression at synapses, endocannabinoid signaling is reported to be involved in the regulation of cell proliferation, migration, differentiation and survival during CNS development (65). However, my morphological investigation revealed no apparent abnormality in gross anatomy of the α-KO and β-KO brains. Furthermore, basal synaptic transmission was normal in the cerebellum and striatum of α-KO and β-KO mice, indicating normal wiring and function of neural circuits. It is possible that the lack of DGLα or DGLβ may be compensated by other signaling molecules during CNS development.

Behavioral studies have clarified the roles of the endocannabinoid system in various brain functions, including acquisition and/or extinction of certain forms of memory, regulation of anxious states, anti-depressant effects, rewarding effects of some addictive compounds, promotion of appetite, relieving pain and protecting neurons (for review, (11, 66)). Many previous studies adopted pharmacological alteration of endocannabinoid signaling and/or local lesions to certain brain structures. However, such manipulations sometimes exert complex effects on animals' behaviors and thus the results are not necessarily consistent. In this respect, α-KO and β-KO mice will be useful tools for elucidating neural mechanisms underlying the behavioral effects of the

endocannabinoid system. These mouse lines are also useful to clarify distinct roles of anandamide and 2-AG in various aspects of brain functions.

Part2

Introduction

Endocannabinoid traveling backwards to presynaptic terminals, bind to cannabinoid CB_1 receptors, and induce transient or persistent suppression of neurotransmitter release (11, 53, 60). In part 1, I found that 2-AG produced by DGLα is regarded as a major endocannabinoid that mediate retrograde signaling at central synapses. Previous studies have clarified detailed subcellular localizations of 2-AG-producing molecules including mGluRs (67), $G_{q/11}$ (45), PLCβs (47) and DGLα (36, 44, 58, 59, 68). These molecules are essentially targeted to dendritic spines on which glutamatergic excitatory synapses are formed, suggesting that 2-AG is efficiently produced by excitatory synaptic activity (54). However, CB_1 receptor expression is generally higher at inhibitory synapses than at excitatory synapses in various brain regions (58, 62). Thus, specificity and efficiency of 2-AG-mediated retrograde synaptic suppression are thought to depend not only on the expression level of CB_1 receptors at presynaptic terminals but also on the distance from the postsynaptic 2-AG production sites to the CB_1 receptors on presynaptic terminals (36, 44, 58, 59, 69). 2-AG-mediated retrograde signaling is generally determined by the balance between the production and clearance of 2-AG. About 85 % of 2-AG is reported to be degraded by a serine hydrolase, MGL (19). Amount of 2-AG

in the brain is markedly increased in global MGL knockout (MGL-KO) mice (70, 71). Depolarization-induced suppression of inhibition/excitation (DSI/DSE) due to Ca^{2+}-ER and mGluR1-mediated synaptic suppression due to basal RER are significantly prolonged in the hippocampus and cerebellum after treatment of MGL inhibitors (41, 72, 73) or in global MGL-KO mice (74, 75). These lines of evidence indicate that MGL significantly contributes to the regulation of 2-AG signaling. Since MGL is found in the cytoplasm of presynaptic terminals (73, 76, 77), it is thought that 2-AG is degraded in a "synapse-specific" manner within the cytoplasm of nerve terminals at which 2-AG suppresses transmitter release by activating CB_1 receptors. However, since not all CB_1-positive nerve terminals express MGL (78), it is unclear whether MGL regulates 2-AG-mediated suppression only at synaptic terminals that express MGL. To address this issue, I used cerebellar PCs that receive two distinct excitatory synaptic inputs, PFs and CFs, and inhibitory inputs from two types of GABAergic interneurons, BCs and stellate cells (SCs). These four types of synapse are known to undergo 2-AG-mediated retrograde suppression following depolarization of PCs (DSE or DSI) (35, 79). I demonstrate that MGL is expressed richly in PF terminals and weakly in Bergmann glia (BG), but is absent in terminals of CFs, SCs, and BCs. In spite of this highly

heterogeneous MGL expression pattern, DSE was significantly prolonged not only at PF-PC synapse but also at CF-PC synapse in global MGL-KO mice and in GC-specific MGL-KO mice. DSE at PF-PC synapses was shortened when MGL was expressed into BG of cultured slices from global MGL-KO cerebellum. Furthermore, in global MGL-KO mice, DSI was significantly prolonged at SC-PC synapses that are surrounded by PFs and located close to BG processes, but not at BC-PC synapses that are remote from MGL-rich PFs. These results suggest that, in the cerebellum, after binding to CB_1 receptors on presynaptic terminals of PF, CF and SC, 2-AG is degraded in a synapse non-specific manner mainly by MGL in PFs and BG.

Materials and Methods

Animals

All experiments were performed according to the guidelines for the care and use of laboratory animals of the University of Tokyo, Hokkaido University and Niigata University. I used global MGL-KO mice, GC-specific MGL-KO mice and their wild-type littermates. Global MGL-KO mice were generated as described previously (78). GC-specific MGL-KO mice were obtained by crossing MGLlox/lox with a E3CreN line (GluN2C+/iCre) whose Cre gene was expressed in GCs under the control of a GluN2C (GluRε3) promoter(80).

Immunohistochemical analyses

Under deep pentobarbital anesthesia (100 mg/kg of body weight), mice at postnatal day 12 (P12), P20-25, and 2 months of age were fixed by transcardial perfusion with 4% paraformaldehyde/0.1M phosphate buffer (PB, pH 7.4) for immunofluorescence microscopy and with 4% paraformaldehyde/0.1% glutaraldehyde/0.1M PB for immunoelectron microscopy. Slices (50 μm in thickness) were cut with a vibratome (VT1000S; Leica). All immunohistochemical incubations were performed by free-floating method at room temperature. Primary antibodies used in the present study

were the same as used in our previous studies(36, 78, 80): guinea pig angti-cannabinoid CB1 receptor (CB1) (22), goat anti-carboinc anhydrase-8 (Car8), rabbit anti-diacylglycerol lipase α (DGLα) (44), goat anti-glutamate/aspertate transporter (GLAST), rabbit anti-metabotropic glutamate receptor type 1α (mGluR1α)(45), guinea pig anti-phospholipase C β4 (PLCβ4) (47), rabbit anti-MGL, goat anti-vesicular glutamate transporter type 1 (VGluT1), guinea pig vesicular glutamate transporter type 2 (VGluT2), and guinea pig anti-vesicular inhibitory amino acid transporter (VIAAT). For immunofluorescence microscopy, I adopted the two steps method to avoid cross immunoreaction of anti-MGL antibody(78). Slices were successively incubated as follows: the first detection with 10% donkey normal serum (20 min), a rabbit MGL antibody (overnight), and a Cy3-labeled rabbit-specific secondary antibody (Jackson ImmunoReseach, 2 hr), and the second detection with 10% rabbit normal serum (20 min), non-rabbit primary antibodies (5 hr), and Alexa488- or Cy5-labeled species-specific secondary antibodies (Invitrogen; Jackson ImmunoResearch, 2 hr). Phosphate buffer saline (PBS) was used as washing and dilution buffers. Fluorescent images were taken with a confocal laser scanning microscope (FV1000; Olympus) equipped with HeNe/Ar laser, and PlanApo (10x/0.40) and PlanApoN (60x/1.42, oil

iersion) objective lens (Olympus). To avoid crosstalk between multiple fluorophores, Alexa488, Cy3, and Cy5 fluorescent signals were acquired sequentially using the 488 nm, 543 nm, and 633 nm excitation laser lines. Single optical sections were obtained (640 x 640 pixels, pixel size 110 nm). For immunoelectron microscopy, slices were successively incubated in 5% bovine serum albumin (BSA)/0.02% saponin/PBS for 30 min, primary antibody diluted in 1% BSA/0.004% saponin/PBS overnight, and 1.4 nm gold particle-conjugated secondary antibody (Nanogold; Nanoprobes) diluted in 1% BSA/0.004% saponin/PBS for 2 hr. After incubation with 2% glutaraldehyde/PBS, gold particles were intensified with the silver enhancement kit (HQ silver; Nanoprobes). Slices were post-fixed with 1% osmium tetroxide, and 2% uranyl acetate, dehydrated, and embedded in Epon812. With an electron microscope (H7100; Hitachi), micrographs were taken randomly from < 5 μm from the surface of the samples to avoid unequal antibody penetration. For statistic analysis, the mean labeling density was calculated from individual micrographs.

Electrophysiological analyses in acute cerebellar slices

Parasaggital slices (250 μm thick) from cerebeller vermis were prepared from mice at postnatal day 8 (P8) to 30 (P30) (for experiments of PF-DSE, CF-DSE and DSI in

global MGL-KO mice, PF-DSE and CF-DSE in GC-specific MGL-KO mice)(27, 81). The standard external solution contained (in mM) 125 NaCl, 2.5 KCl, 2 CaCl2, 1 MgSO4, 1.25 NaH2PO4, 26 NaHCO3, and 20 glucose, bubbled with 95 % O2 and 5 % CO2 (pH 7.4). A recording chamber was perfused with the external solution supplemented with 100 μM picrotoxin (for recording EPSCs) or with 10 μM 2,3 – Dioxo – 6 – nitro – 1,2,3,4 – tetrahydrobenzo quinoxaline – 7 sulfonamide (NBQX) and 10 μM (R) – CPP (for recording IPSCs). For experiments of CF-DSE in GC-specific MGL-KO mice, to improve the voltage clamp of CF mediated EPSC at holding potential of -70 mV, I lowered external Ca2+ concentration to 0.5 mM and increased Mg^{2+} concentration to 2.5 mM.

Whole-cell recordings were made from visually identified PCs at 32 °C using an upright microscope (BX50WI; Olympus, Tokyo, Japan). Patch pipettes (2-3 MΩ) were filled with either of the following solutions containing (in mM): (1) 140 CsCl, 1 EGTA, 10 HEPES, 4.6 MgCl2, 0.1 CaCl2, 4 Na2ATP and 0.4 Na2GTP (pH 7.3, adjusted with CsOH) for the DSE experiments, or (2) 30 CsCl, 110 D-gluconate, 1 EGTA, 10 HEPES, 4.6 MgCl2, 0.1 CaCl2, 4 Na_2ATP and 0.4 Na_2GTP (pH 7.3, adjusted with CsOH) for DSI experiments. Membrane currents were recorded with an EPC-9/2 amplifier (HEKA

Electronik, Lambrecht/Pfalz, Germany). The signals were filtered at 3 kHz and digitized at 20 kHz. Holding potentials of PCs were -70 mV. The pipette access resistance was compensated by 80 %. During baseline recording for at least 1 min, PFs and CFs were stimulated at 0.2 Hz, whereas putative interneuron axons were stimulated at 0.33 Hz. DSE was estimated as the average of two consecutive EPSC amplitudes after the depolarization relative to the baseline EPSC amplitude for 60 s before the depolarization. DSI was estimated as the percentage of the mean amplitude of three consecutive IPSCs after the depolarization relative to the baseline IPSC amplitude for 60 s before the depolarization (79).

Organotypic slice culture

The methods for culture of the cerebellum were similar to those described previously for thalamo-cortical cultures (82). Briefly, cerebellar slices of 250 μm thickness were dissected from the vermis of MGL-KO mice at P9 or P10 that were deeply anaesthetized with isoflurane under a dissecting microscope. The cerebellar slice was placed on a membrane filter (Millicell-CM PICMORG50, MILLIPORE, Bedford, MA, USA), which was coated with rat-tail collagen. The culture medium contained 2.5% HBSS and 22.5% milliQ with B27 supplements instead of 25% HBSS were used. These

cultures were maintained at 37 oC in an environment of humidified 95% air and 5% CO2. One-half of the culture medium was exchanged with fresh medium every other day. The level of the medium was adjusted slightly below the surface of the explants so that they could receive a sufficient supply of the culture medium and the mixed gas.

Virus preparation and infection

VSV-G pseudotyped lentiviral vectors, pLenti7.3/V5 (Invitrogen, Corporation, Carlsbad, CA) were used in this study. Full-length cDNA of mouse MGL was cloned by PCR with primers (5'- GGAATGCAAAAGCCAAGACTA -3' and 5'-CAGCATGTTGAGGGTGGACACC-3') and subcloned into pLenti7.3/V5 vector (pLenti7.3-MGL/EGFP). The vector was designed to express green fluorescent protein and MGL. A control vector, which expresses only GFP was also constructed (pLenti7.3-EGFP). The Virus vectors were produced by cotransfection of human embryonic kidney 293 T cells (2–6x106/a dish) with a mixture of two packaging plasmids (8 μg of pCMV ΔR8.74 & 3 μg of pMD.G (generous gift by Dr. Karl Deisseroth) and one lentivirus vector (10 μg of pLenti7.3-MGL/EGFP or (pLenti7.3-EGFP) using a calcium phosphate precipitation method as reported previously(83). Briefly, slices were cultured in Dulbecco's modified Eagle's medium

(Gibco, Life Technologies, Grand Island, NY, USA) supplemented with 10% fetal bovine serum (FBS; Clontech, Mountain View, CA), 100 U/mL penicillin G, and 0.1 mg/mL streptomycin (pH 7.35) at 37°C in a 5% CO2 atmosphere. Sixteen hours after transfection, the culture medium was exchanged with fresh medium. The medium containing vector particles was harvested at 40 h after transfection. The medium samples were filtered through 0.22 μm membranes and centrifuged at 27,000 r.p.m. for 90 mins. The virus samples were finally suspended in 30 μl of culture medium (pH 7.4) and stored at 4 °C. PCs were infected by adding directly on the slices the volume of viral stock corresponding to 0.2-1 x 105 TU (0.5 μl) per a coculture with microsyringe with a 33-gauge needle (ITO CORPORATION, Shizuoka, Japan).

Electrophysiological analyses in organotypic slice cultures

Electrophysiological experiments started at day in vitro 7 (DIV 7). Slice cultures were recovered for at least 30 min at room temperature in a reservoir chamber bathed with the solution of the following composition (in mM): 125 NaCl, 2.5 KCl, 2 CaCl2, 1 MgSO4, 1.25 NaH2PO4, 26 NaHCO3, and 21 glucose bubbled with 95% O2 and 5% CO2. The recording chamber was continuously perfused with oxygenated bath solution supplemented with picrotoxin (100 μM) to block inhibitory synaptic transmission.

Kynurenic acid (0.5 μM) was also added to inhibit spontaneous EPSCs originated from granule cells. Whole-cell recordings were made from visually identified or GFP positive PCs using an upright and a fluorescence microscope at 24 °C. The resistance of patch pipettes was 2-4 MΩ when filled with the solution (1). PFs were stimulated at a distance of 50-100 μm from the PC soma in the molecular layer.

Statistics

Statistical significance was assessed by Mann-Whitney U-test for two independent samples. For comparison of multiple samples, one-way ANOVA with Fisher LSD post hoc test was used.

Results

MGL is expressed richly in PF terminals and weakly in BG

I began by examining cellular and subcellular distribution of MGL in the cerebellar cortex at postnatal day 12 (P12) and 60 (P60) by immunohistochemistry (Figure 13). The specificity of MGL antibodies has been verified by blank labeling in global MGL-KO brains in our previous studies (68, 78). By double immunofluorescence for MGL and carbonic anhydrase 8 (Car8), a marker of PCs (38), punctate MGL labeling was prominent in the neuropil of the molecular layer (ML), but was absent in Car8-labeled PC dendrites and somata (Figure 13A). Bright MGL puncta in the ML were often overlapped with small boutons that were immunopositive for type 1 vesicular glutamate transporter (VGluT1), a marker of parallel fiber (PF) terminals (arrowheads in Figure 13B) (84). I also noted faint MGL signals in the neuropil, which were not overlapped with, but distributed around VGluT1-positive PF terminals. These MGL signals were found to overlap with signals of GLAST, a glial glutamate transporter particularly rich in BG (Figure 13C) (85). By marked contrast, no immunoreactivity for MGL was detected in large boutons that were immunopositive for type 2 vesicular glutamate transporter (VGluT2), a marker for CF terminals (arrows in

Figure 13B) (84). MGL immunoreactivity was also absent in GABAergic terminals of ML interneurons on the soma and dendrites of PCs, which were labeled with the antibody against vesicular inhibitory amino acid transporter (VIAAT) (Figure 13D). By preembedding immunogold electron microscopy in the adult cerebellum, metal particles for MGL were distributed intracellularly in PF terminals forming asymmetrical synapses with PC spines (Figure 13E). In addition, labeling was observed in thin lamellate processes of BG (Figure 13E). In contrast, metal particles were rarely detected inside CF terminals (Figure 13F), interneuron terminals (Figure 13G), or PC spines, dendrites, and somata (Figures 13E-G). The density of MGL labeling was calculated as the mean number of metal particles per 1 μm^2 of each element in wild-type and global MGL-KO mice. Statistically significant MGL labeling was found only in PF terminals and BG (Figure 13H). Notably, the density in PF terminals was 2.6 times higher than that of BG (Figure 13H). Together, these immunohistochemical results demonstrate that MGL is expressed strongly in PF terminals and weakly in BG processes, but is absent in CF, SC, and BC terminals.

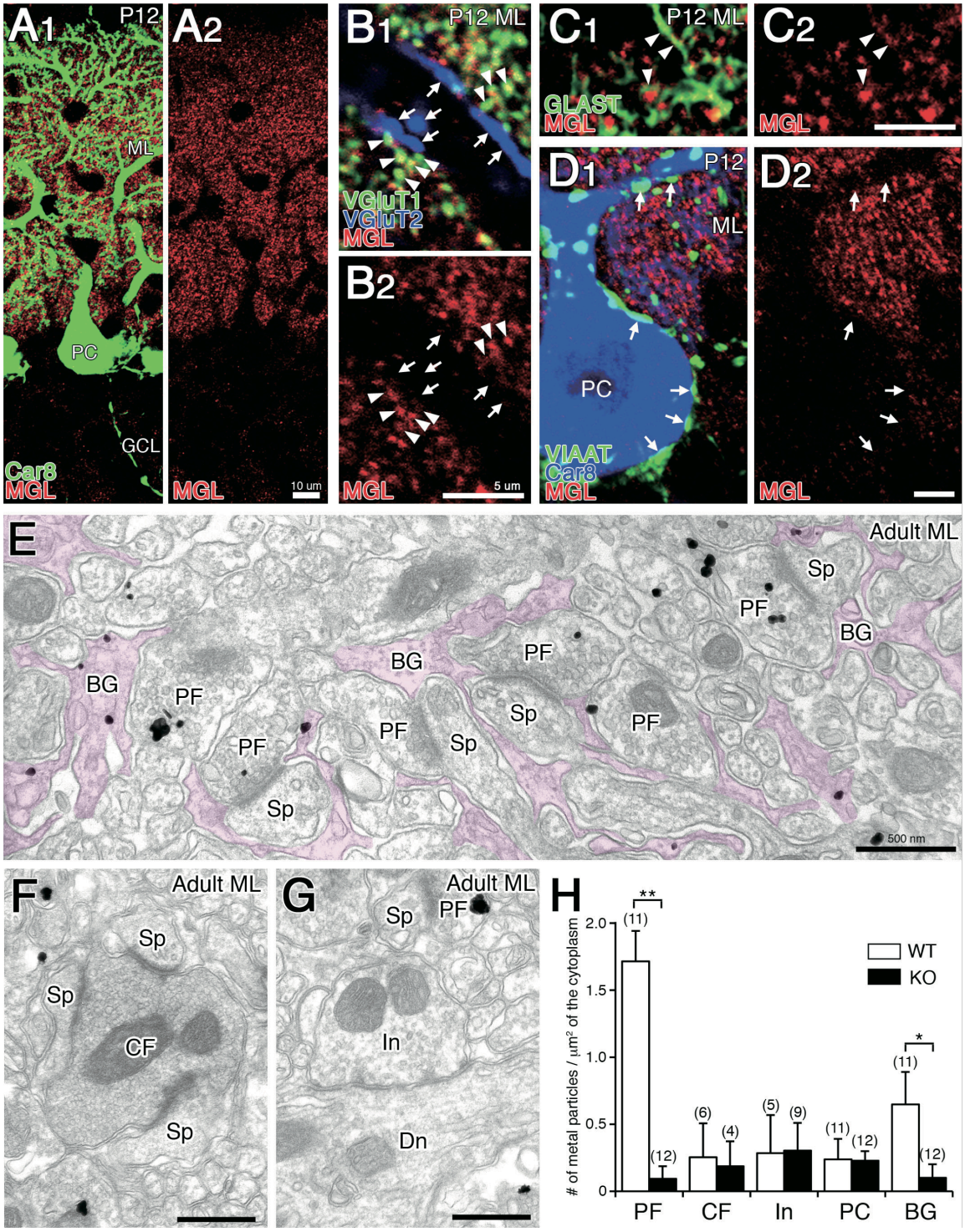
A1
P12
ML
PC
GCL
Car8
MGL
A2
MGL
10 um
B1
P12 ML
VGluT1
VGluT2
MGL
B2
MGL
5 um
C1
P12 ML
GLAST
MGL
C2
MGL
D1
P12
ML
PC
VIAAT
Car8
MGL
D2
MGL
E
Adult ML
BG
PF
PF
BG
PF
Sp
PF
PF
Sp
Sp
Sp
PF
BG
Sp
500 nm
F
Adult ML
Sp
Sp
CF
Sp
G
Adult ML
Sp
PF
In
Dn
H
# of metal particles / μm² of the cytoplasm
2.0
1.5
1.0
0.5
0
**
*
(11)
(12)
(6)
(4)
(5)
(9)
(11)
(12)
(11)
(12)
WT
KO
PF
CF
In
PC
BG

Figure 13. Localization of MGL in the cerebellar cortex. (**A**-**D**) Immunofluorescence for MGL in the cerebellum of P12 mice. (**A**) Double immunofluorescence for MGL and a PC marker, Car8, showing prominent MGL labeling in the neuropil of the ML (ML) and its negativity in Car8-labeled PCs. GCL, granule cell layer. (**B**) Triple immunofluorescence for MGL, VGluT1, and VGluT2 showing strong MGL labeling in VGluT1-labeled PF terminals (arrowheads) but not in VGluT2-labeled CF terminals (arrows). (**C**) Double immunofluorescence for MGL and GLAST showing weak MGL labeling in GLAST-positive BG (arrowheads). (**D**) Triple immunofluorescence for MGL, Car8 and vesicular inhibitory amino acid transporter (VIAAT) showing no immunoreactivity for MGL in VIAAT-labeled interneuron terminals (arrows) located on the surface of Car8-labeled PC dendrites and somata. (**E**-**H**) Preembbedding silver-enhanced immunogold for MGL in the adult (2 months of age) cerebellum showing intracellular MGL labeling in PF terminals (**E**, **G**) and BG processes (BG, colored in purple, **E**), but not in CF terminals (**F**), interneuron terminals (In, **G**), or PC spines (Sp, **E**-**G**) and dendrites (Dn, **G**). (**H**) Summary bar graph demonstrates the mean number of metal particles per 1 μm^2 of each element of WT and global MGL-KO mice. The number above each column indicates the number of electron micrographs used for statistical analysis. Error bars represent s.e.m. Scale bars: 10 μm (**A**), 5 μm (**B**-**D**); 500 nm (**E**-**G**). *$p < 0.05$, **$p < 0.01$ (Mann-Whitney U test).

MGL expressed in PF terminals facilitates termination of CF-DSE.

Then I examined how genetic deletion of MGL affected endocannabinoid-mediated retrograde synaptic suppression in the cerebellum. A recent study showed that DSE at PF-PC and CF-PC synapses were prolonged in global MGL-KO mice (75). I confirmed that both PF-DSE and CF-DSE were significantly prolonged in global MGL-KO mice when compared to their WT littermates (Figures 14 A-F) with no changes in presynaptic CB_1 receptor sensitivity (Figure 14G), depolarization-induced Ca^{2+} transients (Figure 14H), basic properties of synaptic transmission (Table 2), and expression and localization of key molecules for retrograde 2-AG signaling (mGluR1α, PLCβ4, DGLα, CB_1) (Figure 15).

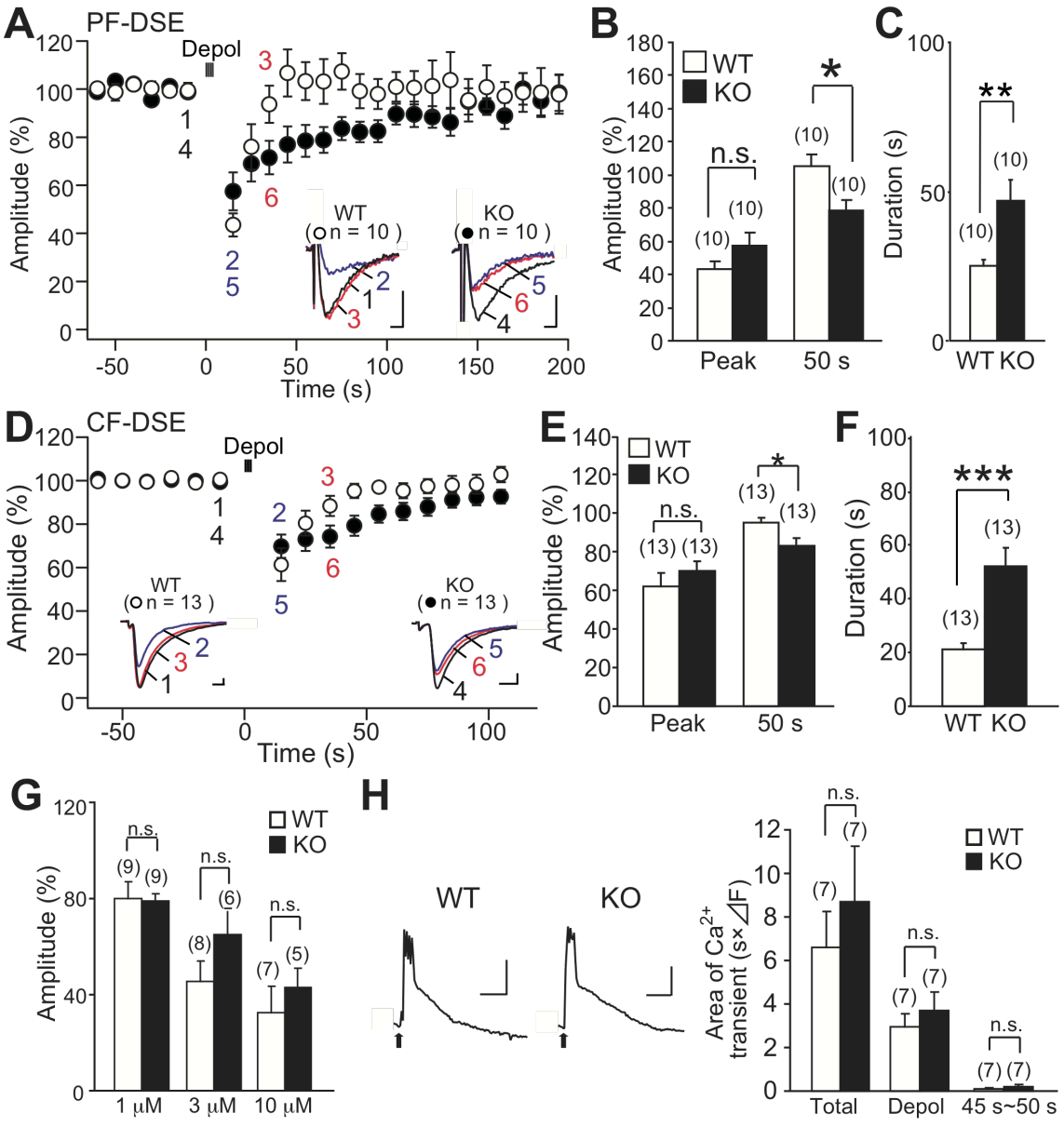
A
PF-DSE
Depol
Amplitude (%)
Time (s)
WT
(n = 10)
KO
(n = 10)
B
WT
KO
n.s.
*
(10)
Peak
50 s
C
**
Duration (s)
WT KO
D
CF-DSE
Depol
Amplitude (%)
Time (s)
WT
(n = 13)
KO
(n = 13)
E
WT
KO
n.s.
*
(13)
Peak
50 s
F
***
Duration (s)
WT KO
G
WT
KO
n.s.
Amplitude (%)
1 μM
3 μM
10 μM
H
WT
KO
Area of Ca2+ transient (s×⊿F)
Total
Depol
45 s~50 s

Figure 14. The 2-AG-mediated suppression is prolonged at PF-PC and CF-PC synapses in global MGL-KO mice.

(**A** and **D**) Sample traces and averaged time courses of PF-mediated EPSCs (**A**) and CF-mediated EPSCs (**D**) from PCs of WT (open circles, P12 – P20) and global MGL-KO (KO) (closed circles, P8 – P12) mice before and after five depolarizing pulses (100ms duration, from -70 mV to 0 mV, repeated at 1 Hz). Traces obtained before (1, 4), 5 – 10 s after (2, 5) and 40 – 45 s after (3, 6) the depolarization pulses are superimposed. (**B** and **E**) Summary bar graphs showing the maximum magnitude of PF-DSE (**B**) and CF-DSE (**E**) at 5 – 10 s after (Peak) and 45 – 50 s after (50 s) depolarization. In **B**, **C**, **E** and **F**, the number of cells for each experiment is indicated in parenthesis. Calibration bars: 0.1 nA and 5 ms for **A** WT, 50 pA and 5 ms for **A** KO, 1 nA and 5 ms for **D** WT, 0.2 nA and 2 ms for **D** KO. Data are presented as mean ±SEM. *$p < 0.05$, **$p < 0.01$, ***$p < 0.001$ (Mann-Whitney *U* test).

(**G** and **H**) Cannabinoid sensitivity at PF-PC synapses and depolarization-induced Ca^{2+} transients in PCs are normal in global MGL-KO mice. (**G**) Summary bar graphs showing the magnitude of presynaptic suppression of PF-EPSCs induced by the CB_1 agonist WIN55, 212-2. The concentration of WIN55, 212-2 is indicated below each set of columns. (**H**) Representative traces (left) and summary bar graphs for the area of Ca^{2+} transients elicited by depolarizing pulses to PCs. The number of cells for each experiment is indicated in parenthesis. Calibration bars: 0.2 $\Delta F/F$ and 10 s for **B**. n.s., not significant.

		WT	KO
10 - 90 % Rise Time (ms)	CF-EPSC	0.49 ± 0.03 (n = 12)	0.57 ± 0.05 (n = 18)
	PF-EPSC	1.12 ± 0.11 (n = 9)	1.11 ± 0.08 (n = 9)
	IPSC (BC-PC)	0.74 ± 0.04 (n = 13)	0.71 ± 0.04 (n = 13)
	IPSC (SC-PC)	1.39 ± 0.24 (n = 6)	1.28 ± 0.13 (n = 7)
Decay Time Constant (ms)	CF-EPSC	2.56 ± 0.22 (n = 12)	3.44 ± 0.36 (n = 18)
	PF-EPSC	6.70 ± 1.02 (n = 9)	5.38 ± 0.45 (n = 9)
	IPSC (BC-PC)	3.36 ± 0.41 (n = 13)	2.64 ± 0.15 (n = 13)
	IPSC (SC-PC)	3.30 ± 0.45 (n = 6)	3.65 ± 0.31 (n = 7)
Paired - Pulse Ratio (2_{nd} / 1_{st})	CF-EPSC	0.38 ± 0.06 (n = 12)	0.34 ± 0.04 (n = 18)
	PF-EPSC	1.60 ± 0.08 (n = 9)	1.53 ± 0.06 (n = 9)
	IPSC (BC-PC)	0.77 ± 0.06 (n = 13)	0.74 ± 0.03 (n = 13)
	IPSC (SC-PC)	0.91 ± 0.09 (n = 6)	0.63 ± 0.13 (n = 7)

Table 2. Rise time, decay time constant and paired-pulse ratio of synaptic currents in WT and global MGL-KO mice.

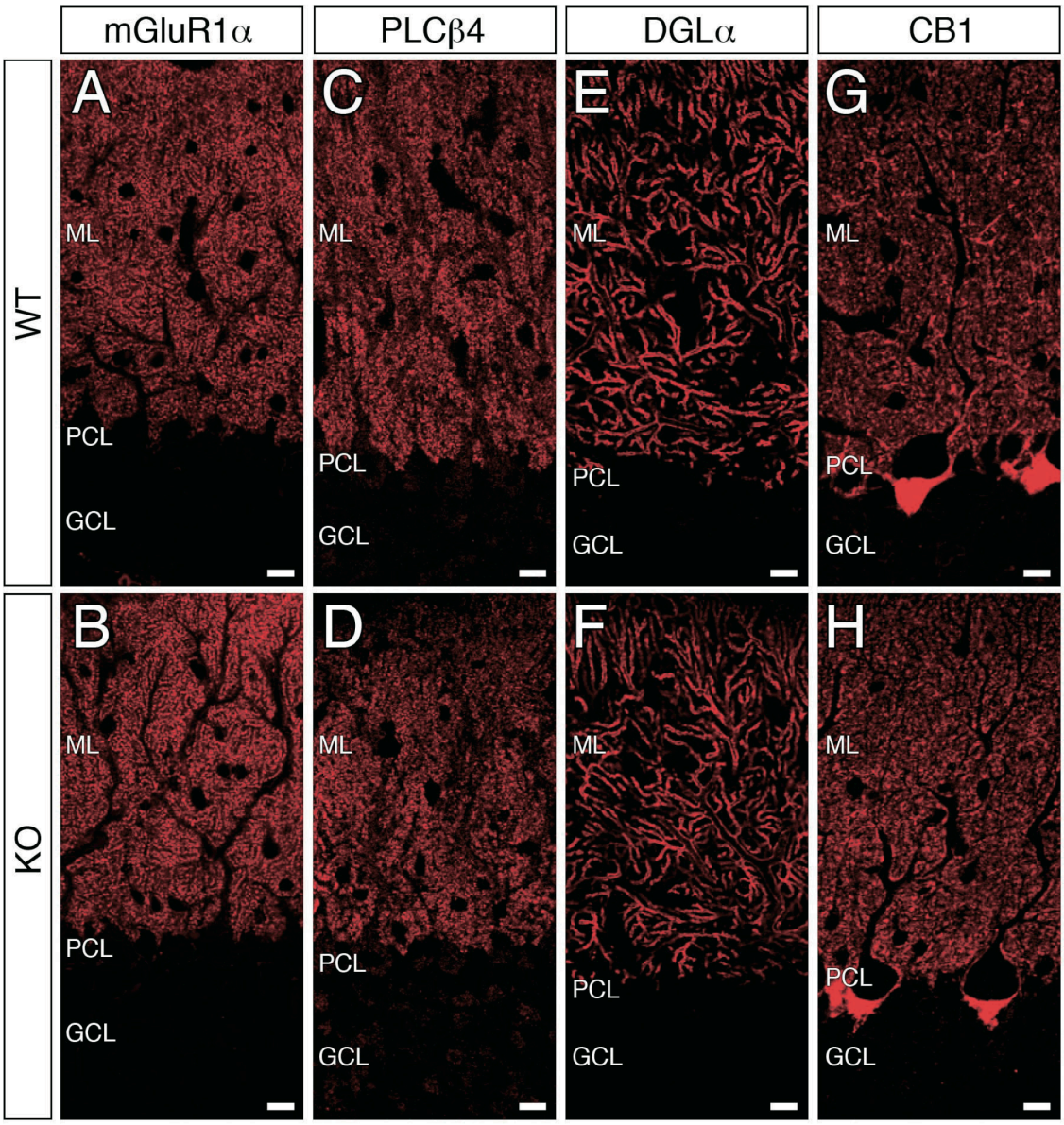

Figure 15. Expression and localizations of the 2-AG-signaling molecules are normal in global MGL-KO mice. Immunofluorescence for mGluR1α (**A** and **B**), PLCβ4 (**C** and **D**), DGLα (**E** and **F**) and CB_1 (**G** and **H**) in the cerebellum of WT (**A**, **C**, **E** and **G**) and global MGL-KO (**B**, **D**, **F** and **H**) mice. There were no differences in the expression and localization of these molecules between WT and global MGL-KO mice. ML, molecular layer; PCL, Purkinje cell layer; GCL, granule cell layer. Scale bar, 10 mm.

These results on global MGL-KO mice raise a question why DSE is prolonged at CF-PC synapses where no MGL expression was detected in their presynaptic terminals (Figure 13). One possibility would be that MGL, which is expressed strongly in PF terminals and weakly in BG, hydrolyzes 2-AG around CF terminals and regulates the duration of DSE at CF-PC synapse. To clarify the contribution of MGL in PF terminals to the regulation of DSE, I generated mice with GC-specific deletion of MGL (GC-specific MGL-KO mice) and examined DSE at CF-PC and PF-PC synapses. To obtain a GC-specific Cre recombinase expression, I used an E3CreN line ($GluN2C^{+/iCre}$) whose Cre gene was expressed in GCs under the control of a GluN2C (GluRε3) promoter (80). By intercrossing MGL floxed ($MGL^{lox/lox}$) mice with the E3CreN line, I created GC-specific MGL-KO mice. I confirmed that MGL immunoreactivity in the ML was decreased greatly in GC-specific MGL-KO mice when compared with WT mice (Figures 16A, B, D, and E). However, weak signals for MGL remain as compared with global MGL-KO mice (Figures 16B, C, E, and F). Triple immunofluorescent labeling experiments revealed that vGluT1-labeled PF terminals (double arrowheads in Figures 16G-I) exhibited intense immunoreactivity for MGL in WT (Figure 16G3), but not in GC-specific MGL-KO (Figure 16H3) or global MGL-KO (Figure 16I3) mice. By

contrast, GLAST-labeled BG processes (arrowheads in Figures 16G-I) exhibited weak immunoreactivity for MGL in WT (Figure 16G3) and GC-specific MGL-KO mice (Figure 16H3), but not in global MGL-KO mice (Figure 16I3). These results indicate that MGL immunoreactivity was eliminated from PF terminals but present in BG in GC-specific MGL-KO mice.

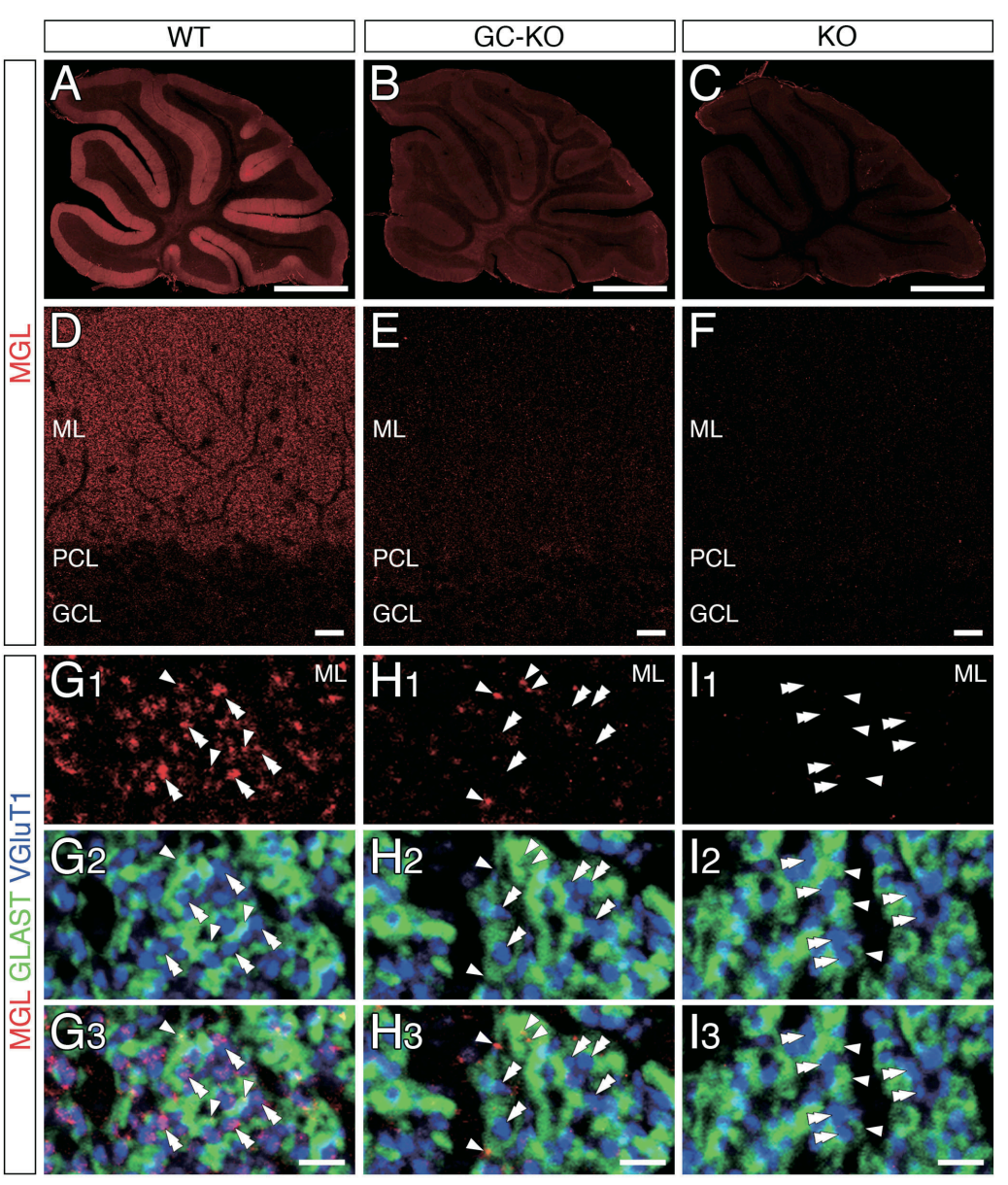

Figure 16. PF-specific deletion of MGL in GC-specific MGL-KO mice

(**A**-**F**) Immunofluorescence for MGL in parasagittal cerebellar sections in WT (**A**, **D**, WT), GC-specific MGL-KO (**B**, **E**, GC-KO), and global MGL-KO (**C**, **F**, KO) mice at P20-25. **D**-**F** are enlarged images in the cerebellar cortex.

(**G**-**H**) Triple immunofluorescence for MGL (red), GLAST (green), and VGluT1 (blue) in the ML of WT, GC-specific MGL-KO, and global MGL-KO mice. Single and double arrowheads depict VGluT1-labeled PF terminals and GLAST-labeled BG processes, respectively. PCL, Purkinje cell layer; GCL, granule cell layer.

Scale bars: 1 mm (**A**-**C**), 20 μm (**D**-**F**), 2 μm (**G**-**I**).

I examined DSE at CF-PC synapse following depolarization of PCs (5 s duration, -70 mV to 0 mV). As shown in Figure 17A, DSE at CF-PC synapse was significantly prolonged in GC-specific MGL-KO mice when compared to WT mice. Interestingly, the DSE prolongation in GC-specific MGL-KO mice was less prominent when compared to global MGL-KO mice (Figure 17A). While the peak magnitudes of DSE measured at 5-10 s after depolarization were similar among the three mouse strains, the DSE magnitude of GC-specific MGL-KO mice at 40-50 s after depolarization was significantly larger than those of WT mice, but significantly smaller than global MGL-KO mice (Figure 17B). Consequently, the duration of DSE measured as the time to reach 50 % recovery from the peak DSE was in the order of global MGL-KO mice, GC-specific MGL-KO mice, and WT mice (Figure 17C). I then examined DSE at PF-PC synapse following depolarization of PCs (3s duration, -70 mV to 0 mV) in the three strains of mice. As shown in Figure 17D, DSE in GC-specific MGL-KO mice was significantly prolonged when compared to WT mice, but recovered significantly faster when compared to global MGL-KO mice (Figure 17D). The magnitude and duration of DSE in GC-specific MGL-KO mice were intermediate between those of WT and global MGL-KO mice (Figures 17E and F). These results indicate that MGL in PF terminals

facilitates termination of 2-AG signaling not only “homosynaptically” at PFs but also “heterosynaptically” at CFs. The difference in DSE duration and magnitude between GC-specific and global MGL-KO mice strongly suggest that MGL present in cerebellar tissues other than PF terminals significantly contributes to the termination of 2-AG signaling. As MGL was present in BG in GC-specific MGL-KO mice (Figure 16H), glial MGL is considered to be important for termination of 2-AG signaling.

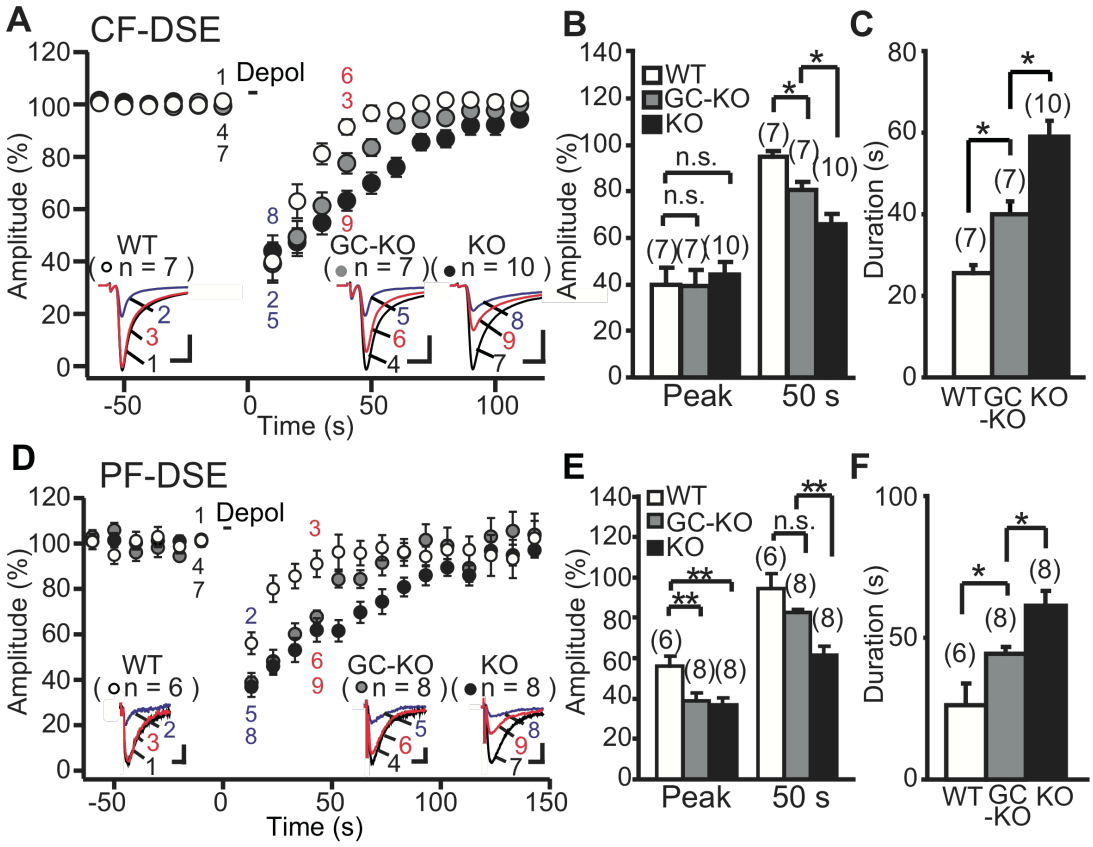

Figure 17. DSE is prolonged at CF-PC and PF-PC synapses in GC-specific and global MGL-KO mice

(**A**, **D**) Sample traces and averaged time courses of CF-EPSCs (**A**) and PF-EPSCs (**D**) from PCs of wild-type (WT) (open circles, P25-P30), GC-specific MGL-KO (GC-KO) (gray circles, P25-P30) and global MGL-KO (KO) (closed circles, P25-P30) mice before and after depolarization. Traces obtained before (1, 4, 7, black), 5-10 s after (2, 5, 8, blue) and 40-45 s after (3, 6, 9, red) depolarization are superimposed. (**B**, **E**) Summary bar graph showing the magnitude of CF-DSE (**B**) and PF-DSE (**E**) at the time points 5-10 s (Peak) and 45-50 s after (50 s) depolarization. (**C**, **F**) Duration of DSE (half width) measured as the time to reach 50 % recovery from the maximum magnitude of DSE. In **B**, **C**, **E**, **F**, **G** and **H**, the number of cells for each experiment is indicated in parenthesis. Calibration bars: 2 nA and 5 ms for (CF-DSE: WT and GC-KO), 1nA and 2 ms for (CF-DSE: KO), 50 pA and 5 ms for (PF-DSE: WT and GC-KO), 0.1 nA and 5 ms for (PF-DSE: KO). Data are presented as means ± s.e.m. *P < 0.05, **P < 0.01 (one-way ANOVA with Fisher LSD multiple comparison post hoc test).

MGL within BG facilitates termination of 2-AG-mediated retrograde signaling

To directly examine whether MGL in BG can influence the termination of 2-AG signaling in the cerebellum, I developed a reduced cerebellar preparation in which MGL was expressed richly in BG but absent in PFs. I made organotipic cerebellar slice cultures from global MGL-KO mice at P9 or P10, and expressed MGL gene into BG by using a lentivirus vector (Figure 18). I confirmed that immunoreactivity of MGL was overlapped with that of GLAST (Figure 18A, upper panel) but not with that of VGluT1 (Figure 18A, lower panel), indicating that MGL was richly expressed in BG. I then made whole-cell recordings from PCs, stimulated PFs in the ML and recorded PF-EPSCs. Slice cultures from global MGL-KO mice with overexpression of GFP alone into BG were used as control. I checked that CB_1 receptor sensitivity was not altered at PF-PC synapses in slice cultures with MGL expression in BG when compared to control slices (Figure 18B).

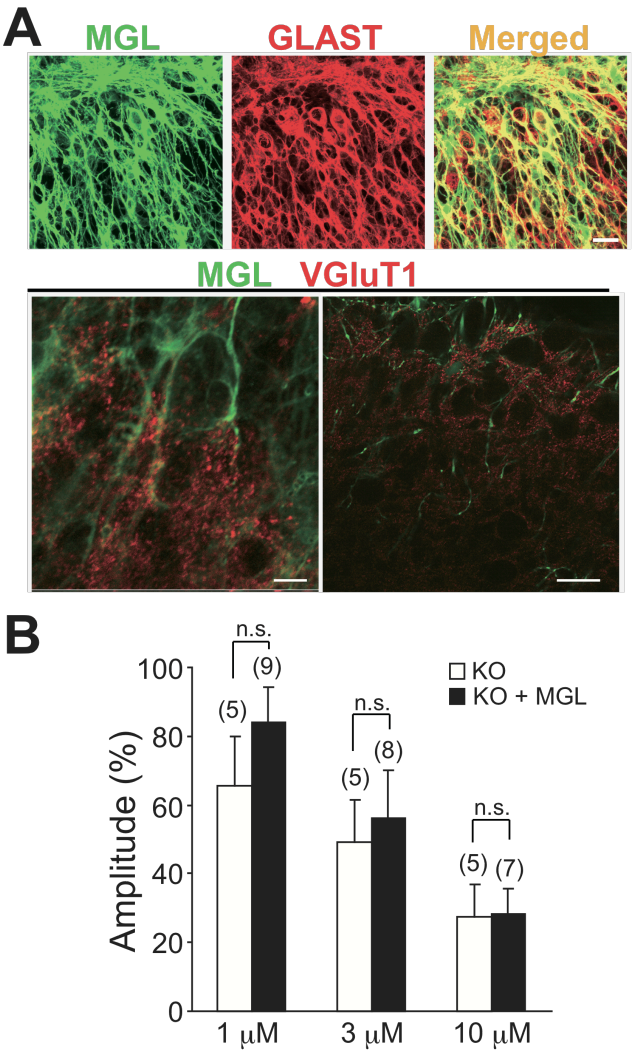

Figure 18. Lentivirus-mediated expression of MGL into the Bergmann glia (BG), but not into PFs, of organotypic cerebellar slices cultures of global MGL-KO mice. (**A**; Upper panel) Colocalization of MGL and GLAST immunoreactivities in cultured cerebellar slices from global MGL-KO mice with lentivirus-mediated expression of MGL. (**A**; Lower panel) MGL (green) and VGluT1 (red) immunoreactivites were not colocalized. Scale bars; 30 mm (Upper panel), 5 μm (Lower panel, left), 30 μm (Lower panel, right). (**B**) Cannabinoid sensitivity at PF-PC synapses is normal in organotypic cerebellar slice cultures from global MGL-KO mice (KO) and from those with lentivirus-mediated expression of MGL into their BG (KO + MGL). Summary bar graphs showing the magnitudes of presynaptic suppression of PF-EPSCs induced by WIN55, 212-2. The concentration of WIN55, 212-2 is indicated below each set of columns. The number of cells for each experiment is indicated in parenthesis (Mann-Whitny *U* test). n.s., not significant.

I then elicited DSE at PF-PC synapse by applying 10 depolarization pulses (100 ms duration, -70 mV to 0 mV, repeated at 1 Hz) to PCs. I found that DSE recovered significantly faster in slice cultures with MGL expression in BG than in control cultures (Figure 19A). Magnitude of DSE at the peak and 130 s after depolarization as well as the duration of DSE were significantly smaller in slice cultures with MGL expression than in MGL-KO cultures (Figures 19B and C). These results suggest that MGL in BG can influence the duration of DSE.

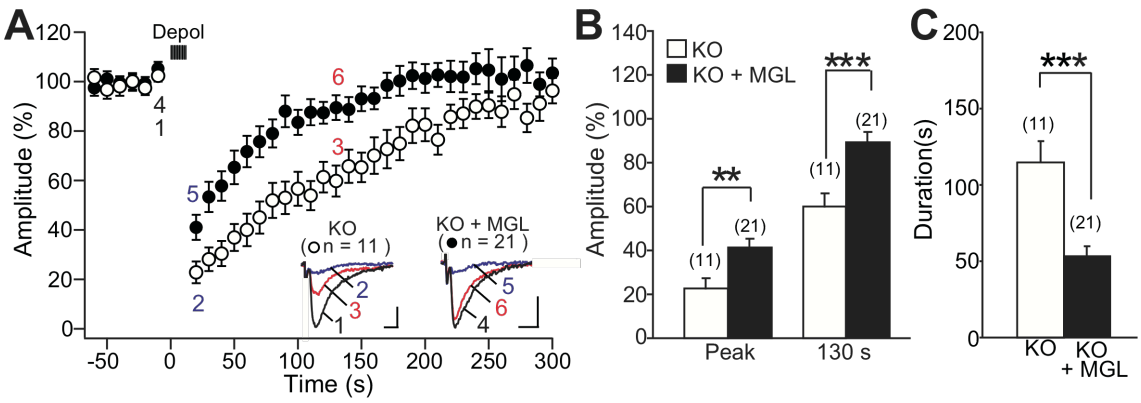

Figure 19. MGL expressed in BG shortens PF-DSE.

(**A**) Sample traces and averaged time courses of PF-EPSCs from PCs in cerebellar slice cultures with overexpression of GFP alone (KO, open circles) or MGL plus GFP (KO + MGL, closed circles) into BG from global MGL-KO mice before and after applying 10 depolarizing pulses to PCs (100 ms duration, from -70 mV to 0 mV, repeated at 1 Hz). Traces obtained before (1, 4, black), 5-10 s after (2, 5, blue) and 125-130 s after (3, 6, red) depolarization are superimposed.

(**B** and **C**) Summary bar graph showing the magnitude (**B**) and duration (**C**) of PF-DSE illustrated similarly to Figure 17. Calibration bars: 0.1 nA and 5 ms. Data are presented as means ± s.e.m. *p < 0.05, **p < 0.01, ***p < 0.001 (Mann-Whitney *U*-test).

MGL facilitates termination of DSI at SC-PC synapses

The results so far indicate that MGL in PF terminals and BG hydrolyzes 2-AG in a synapse "non-specific" manner and facilitates termination of 2-AG-mediated retrograde signaling at both PF-PC and CF-PC synapses. MGL immunoreactivity is strong in the ML and very weak in PC layer (PCL) and GC layer in the cerebellum (Figures 13A2 and D2). Since CF terminals are surrounded by PF terminals and enwrapped by BG processes, 2-AG around CF terminals is thought to be degraded by MGL in PF terminals and BG. Therefore, spatial disposition of MGL seems to be important for its regulation of 2-AG-mediated retrograde signaling. GABAergic synapses from BCs and SCs to PCs undergo 2-AG mediated transient suppression following depolarization of PCs, a phenomenon known as DSI (42-44). However, GABAergic nerve terminals in the ML and PCL, which represent SC and BC terminals, respectively, do not express MGL (Figures 13D, G, and H). While SCs form GABAergic synapses on PC dendrites that are embedded within a cloud of PF terminals, BCs innervate PC somata that are distant from PF terminals. Therefore, DSI at SC synapses is thought to be influenced more strongly by MGL than DSI at BC synapses. I thus compared DSI at BC and SC synapses between wild-type and global MGL-KO mice.

For differentially stimulating axons of BCs and SCs, I placed stimulation pipettes near the PCL and in the outer half of the ML, respectively (Figure 20A). IPSCs evoked by stimulation near the PCL were thought to arise mostly from BC axons forming synapses on the PC soma, whereas those evoked by stimulation at the outer ML are considered to originate mainly from SC axons contacting PC dendrites (Figure 20A). To estimate the extent of overlap between the activated axons by stimuli at the two sites, I used homo- and hetero-synaptic paired-pulse protocols. When extracellular Ca^{2+} concentration was elevated, paired stimuli delivered to each site individually (homo-synaptic paired stimulation) at 30 ms intervals resulted in clear depression of the second IPSCs (Figure 20B). In contrast, when stimulation at one site was precede by stimulation at the other site at 30 ms interval (hetero-synaptic paired stimulation), no significant depression was observed (Figure 20B). These results indicate that stimuli at the ML and near the PCL activated non-overlapping population of inhibitory axons. Since synaptic currents arising from synapses distant from the somatic recording site undergo stronger distortion and have longer rise times than those arising from the soma (86, 87), I checked the 10 to 90 % rise times of IPSCs to estimate the sites of GABAergic synapses along the somatodendritic domain of PCs. I found that about 90 % of the IPSCs by

stimulation near the PCL had rise times shorter than 0.8 ms, whereas about 90 % of IPSCs by stimulation at the outer ML had rise times longer than 0.6 ms (Figure 20C). To exclude the possible overlap between the two populations, I determined IPSCs with rise times shorter than 0.6 ms as arising from putative BC axons and those with rise times longer than 0.8 ms as being evoked by stimulating putative SC axons.

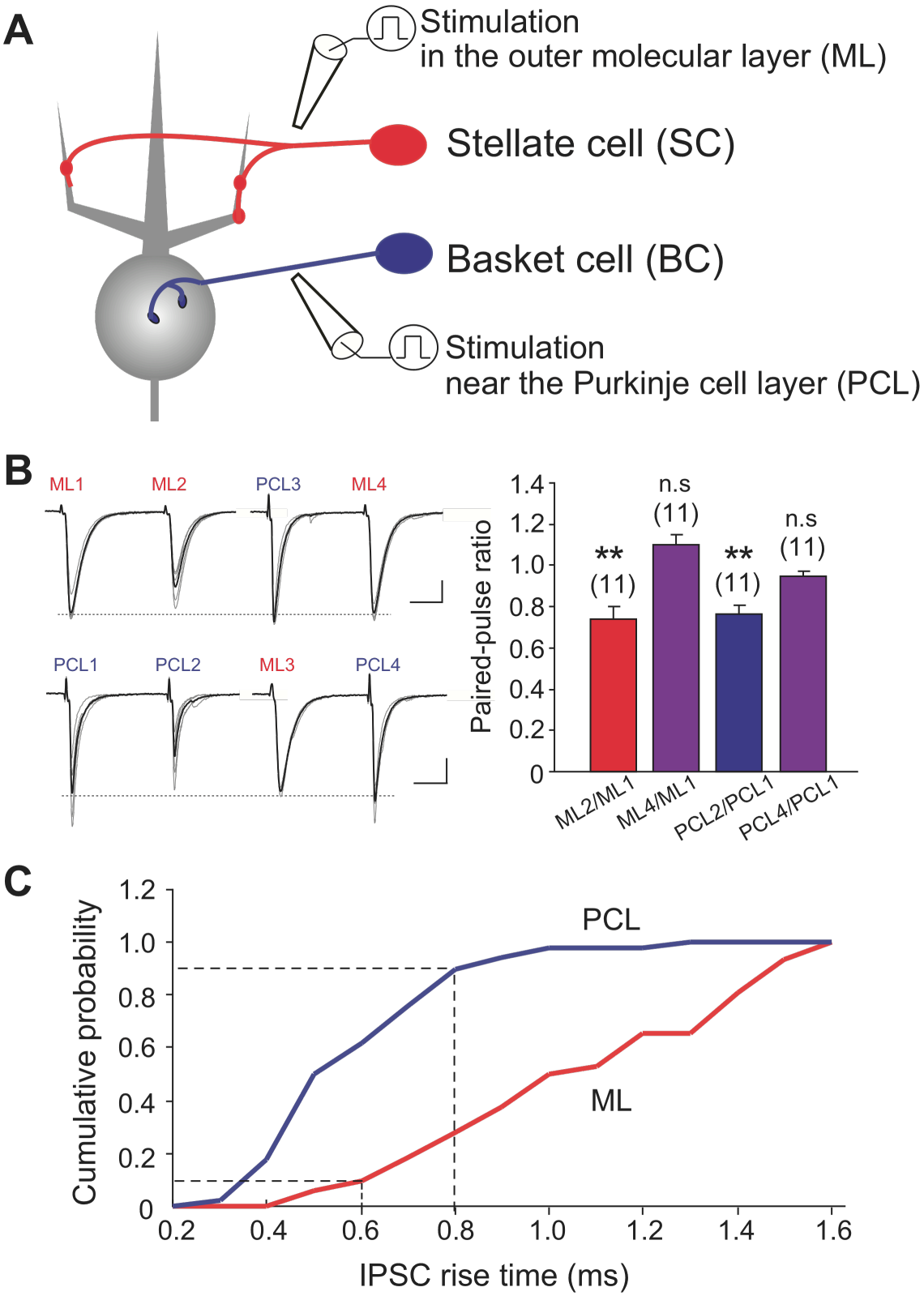
A
Stimulation
in the outer molecular layer (ML)
Stellate cell (SC)
Basket cell (BC)
Stimulation
near the Purkinje cell layer (PCL)
B
ML1
ML2
PCL3
ML4
PCL1
PCL2
ML3
PCL4
Paired-pulse ratio
1.4
1.2
1.0
0.8
0.6
0.4
0.2
0
**
(11)
n.s
(11)
**
(11)
n.s
(11)
ML2/ML1
ML4/ML1
PCL2/PCL1
PCL4/PCL1
C
Cumulative probability
1.2
1.0
0.8
0.6
0.4
0.2
0
PCL
ML
0.2
0.4
0.6
0.8
1.0
1.2
1.4
1.6
IPSC rise time (ms)

Figure 20. Experimental design for Figure 21. (**A**) Schematic drawing showing the arrangement of the stimulation pipettes for evoking IPSCs originating from putative stellate cell (SC) and basket cell (BC) axons, respectively. (**B**) Stimuli in the molecular layer (ML) and those near the PCL activate nonoverlapping populations of inhibitory axons. (left) Sample traces from a representative experiment. Paired stimuli to the same site (ML1 + ML2 or PCL1 + PCL2) resulted in a clear depression of the IPSCs to the second stimuli relative to those to the fist stimuli. When the stimuli at one site (ML4 or PCL4) was presented by those at other site (PCL3 or ML3), no depression was observed. (right) Summary bar graph showing a significant paired-pulse depression when the pairs of stimuli were applied to the same site (ML2/ML1, PCL2/PCL1) but no depression when the stimuli at one site were presented by those at the other site (ML4/ ML1, PCL4/PCL1). Extracellular solution contained 4 mM Ca^{2+} and 0 mM Mg^{2+}, and Hepes (10 mM) was used instead of bicarbonate buffer to adjust pH to 7.3. Calibration bars; 0.5 nA and 10 ms. The number of cells for each experiment is indicated in parenthesis. **$p < 0.01$ (Wilcoxon's signed rank test); n.s., not significant. (**C**) Cumulative histogram of the 10 -90 % rise times of IPSCs elicited by stimulation in the outer molecular layer (red line) and near the PC layer (blue line). Note that about 90 % of the IPSCs by stimulation near the PC layer had rise times shorter than 0.8 ms, whereas about 90 % of IPSCs by stimulation of the outer molecular layer had rise times longer than 0.6 ms. To exclude the possible overlap between the two populations, I determined IPSCs with rise times shorter than 0.6 ms as arising from putative BC axons and those with rise times longer than 0.8 ms as being evoked by stimulating putative SC axons.

I compared DSI by applying 5 depolarizing pulses (100 ms duration, from -70 mV to 0 mV, repeated at 1 Hz) to PCs between WT and global MGL-KO mice. For IPSCs arising from putative SC axons (i.e., rise time > 0.8 ms), DSI was significantly prolonged in global MGL-KO mice when compared to WT mice (Figure 21A). While the peak magnitudes of DSI measured at 5-10 s after depolarization were similar between the two mouse strains, the DSI magnitude of global MGL-KO mice at 40-50 s after depolarization was significantly larger than wild-type mice (Figure 21B). The duration of DSI measured as the time to reach 50 % recovery from the peak DSI was significantly longer in global MGL KO mice than in wild-type mice (Figure 21C). By marked contrast, for IPSCs arising from putative BC axons (i.e., rise time < 0.6 ms), DSI was not prolonged in global MGL-KO mice (Figure 21D). Although the peak magnitude of DSI was greater in global MGL-KO mice, the magnitude at 40-50 s after depolarization and the duration of DSI were not different between wild-type and global MGL-KO mice (Figures 21E and F).

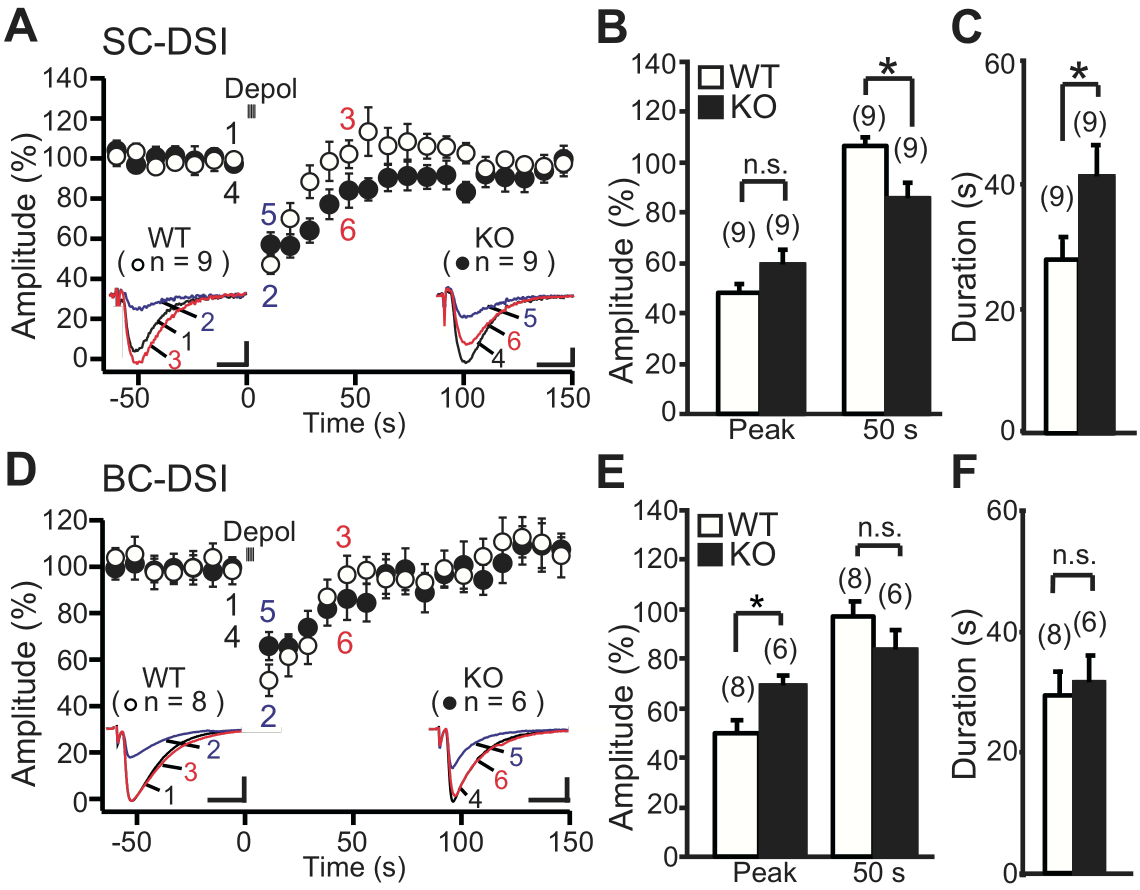

Figsure 21. DSI is prolonged at SC-PC but not BC-PC synapses in global MGL-KO mice.

(**A**, **D**) Sample traces and averaged time courses of IPSCs at putative SC-PC (**A**) and BC-PC (**D**) synapses in wild-type (WT) (open circles, P9-P12) and global MGL-KO (KO) (closed circles, P9-P12) mice before and after 5 depolarization pulses (100 ms duration, from -70 mV to 0 mV, repeated at 1 Hz). Traces obtained before (1, 4, black), 5-10 s after (2, 5, blue) and 45-50 s after (3, 6, red) depolarization are superimposed. (**B**, **C**, **E** and **F**) Summary bar graph showing the magnitude (**B**, **E**) and duration (**C**, **F**) of DSI illustrated similarly to Figure 17.

Calibration bars: 0.1 nA and 5 ms for (**A**) and 0.5 nA and 5 ms for (**D**). Data are presented as means ± s.e.m. *p < 0.05, **p < 0.01 (Mann-Whitney *U*-test).

I also examined whether pharmacological blockade of MGL in WT mice had the same effects on the two types of IPSCs. Incubation of slices with the MGL inhibitor *N*-arachidonoyl maleimide and 4-nitrophenyl 4-(dibenzo[d][1,3]dioxol-5-yl(hydroxy)methyl)piperidine-1-carboxylate (JZL 184) (88) (100 nM) caused a significant prolongation of DSI at putative SC-PC synapses (Figures 22A, B, and C) but had no significant effect on DSI at putative BC-PC synapses (Figures 22D, E, and F).

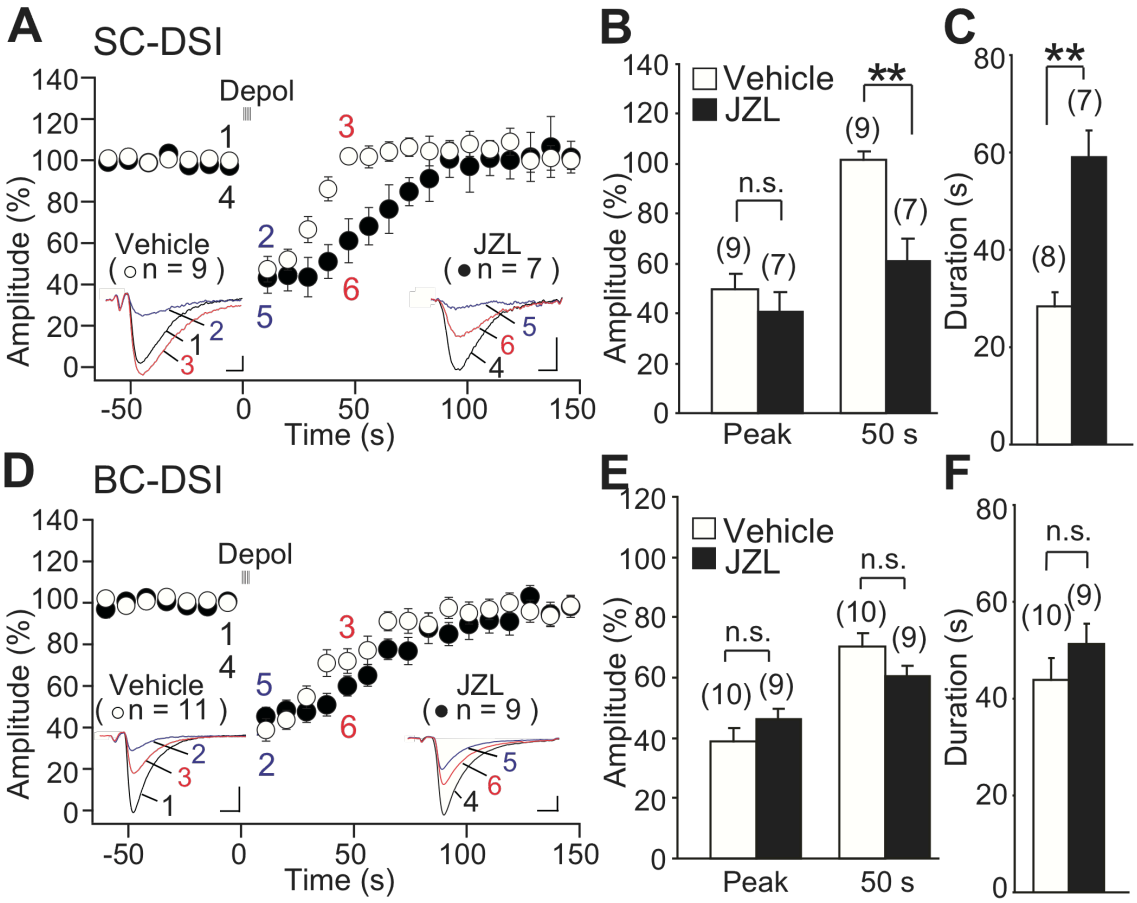

Figure 22. DSI is prolonged at SC-PC but not BC-PC synapses after treatment of the MGL inhibitor JZL. (**A** and **D**) Sample traces and averaged time courses of IPSCs at putative SC-PC (**A**) and BC-PC (**D**) synapses in slices treated with vehicle (open circles, P9 – P12) and JZL184 (closed circles, P9 – P12). Traces obtained before (1, 4, black), 5 – 10 s after (2, 5, blue) and 45 – 50 s after (3, 6, red) the five depolarizing pulses (100 ms duration, from -70 mV to 0 mV, repeated at 1Hz) are superimposed. (**B**, **C**, **E**, and **F**) Summary bar graph showing the magnitude (**B** and **E**) and duration (**C** and **F**) of DSI illustrated similarly to Figure 21. Calibration bars: 0.2 nA and 2 ms for **A** and 1 nA and 2 ms for **D**. Data are presented as means ± SEM. **p < 0.01 (Mann-Whitney *U* test). n.s., not significant.

Finally, I examined whether other endocannabinoid degradation enzymes, α/β-hydrolase domain 6 (ABHD6) and fatty acid amide hydrolase (FAAH), contributed to the time course of DSI at putative BC-PC synapses. Incubation of slices from global MGL-KO mice with the ABHD6 inhibitor *N*-methyl-N-[[3-(4-pyridinyl)phenyl]methyl]-4'-(aminocarbonyl)[1,1'-biphenyl]-4-yl ester, carbamic acid (WWL70) (10 μM) and the FAAH inhibitor 3'-(aminocarbonyl)[1,1'-biphenyl]-3-yl)-cyclohexylcarbamate (URB597) (1μM) had no effect on DSI at putative BC-PC synapses (Figure 23). Together, these results indicate that MGL is important for the termination of DSI at SC-PC synapses whereas none of the three endocannabinoid degradation enzymes contribute significantly to shaping DSI at BC-PC synapses.

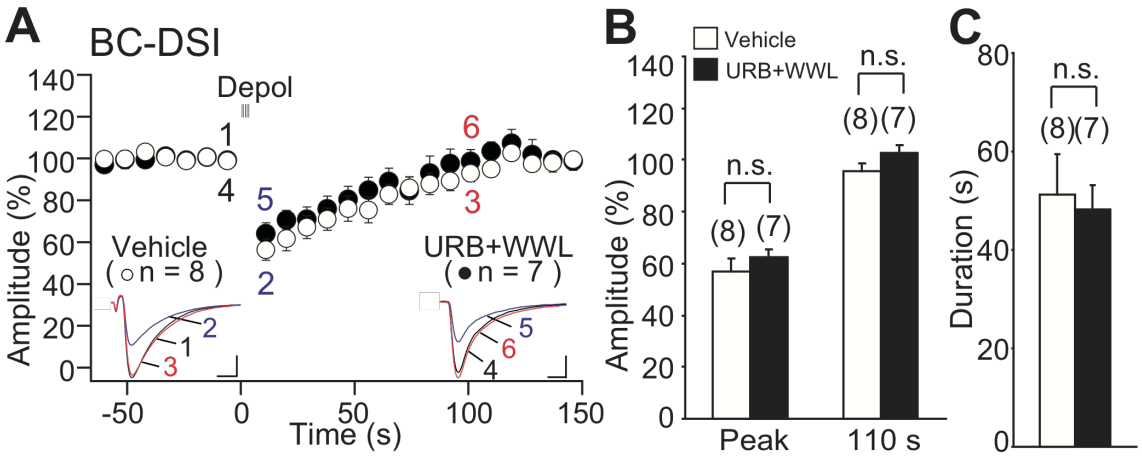

Figure 23. DSI at BC-PC synapses of global MGL-KO mice is not affected by addition of the ABHD6 inhibitor WWL70 and the fatty acid amide hydrolase (FAAH) inhibitor URB597. (**A**) Sample traces and averaged time courses of IPSCs at putative BC-PC synapses in slices from global MGL-KO mice treated with vehicle (open circles, P9 – P12) and with WWL70 and URB597 (closed circles, P9 – P12). Traces obtained before (1, 4, black), 5 – 10 s after (2, 5, blue), and 105 – 110 s after (3, 6, red) the five depolarizing pulses (100ms duration, from -70 mV to 0 mV, repeated at 1 Hz) are superimposed. (**B** and **C**) Summary bar graph showing the magnitude (**B**) and duration (**C**) of DSI illustrated similarly to Figure 21. Calibration bars: 2 nA and 2 ms for **A**. Data are presented as means ± SEM. Slices were incubated with the external solution containing URB597 (1 μM) with BSA (0.2 mg/mL) for 40 min. Next, WWL70 (10 μM) was added to the URB597-containing external solution and the slices were further incubated for 20 min.

Discussion

I examined detailed localization of MGL by immunohistochemistry and found that MGL was expressed abundantly in PF terminals and weakly in BG, whereas MGL expression was very low or absent in presynaptic terminals of CF and inhibitory terminals of BCs and SCs. In spite of this highly heterogeneous MGL expression pattern, DSE was significantly prolonged not only at PF-PC synapse but also at CF-PC synapse in global MGL-KO mice. Furthermore, DSE was prolonged both at PF-PC and CF-PC synapses in GC-specific MGL-KO mice in which cerebellar MGL expression was confined to BG. This result indicates that MGL in PFs regulates 2-AG signaling not only "homosynaptically" at PF-PC synapses but also "heterosynaptically" at CF-PC synapses. Importantly, prolongation of DSE in GC-specific MGL-KO mice was less prominent than in global MGL-KO mice, suggesting that MGL in BG also contributes to termination of 2-AG signaling. This notion was supported by the observation that DSE at PF-PC synapses was shortened when MGL was expressed into BG of cultured slices from global MGL-KO cerebellum. I also found that DSI was prolonged at SC-PC synapses but not at BC-PC synapses in global MGL-KO mice. SC terminals are surrounded by PFs and BG processes in the ML, whereas BC terminals are distant from

these structures. Thus, 2-AG, which is released from PCs and causes retrograde suppression of PF-, CF-, and SC-PC synapses, is degraded in a synapse-type independent manner by MGL present in the cytoplasm of PF terminals and BG. 2-AG that acts as a synaptic retrograde messenger is produced exclusively by DGLα (79, 89) that is essentially targeted to dendritic spines (36, 44, 58, 59, 69). In PCs, DGLα is expressed densely at the base of the spine neck and sparsely on the somatodendritic membrane but is excluded from the main body of the spine neck and head (44). On the other hand, CB_1 is highly enriched at perisynaptic region of PFs within 500 nm from the edge of synaptic junction (62), and preferentially accumulated on the synaptic side facing dendritic spines (44). CB_1 is also rich on GABAergic terminals that form synaptic contacts on dendritic shafts and somata (62) with much lower level of DGLα expression when compared to the spine neck and head (44). These molecular arrangements suggest that 2-AG travels a certain distance from its main production site (the base of the spine neck) to its target (CB_1 receptor) on presynaptic terminals of PFs, CFs, or GABAergic axons. Since the ML is packed with PF terminals and BG processes, 2-AG released from PCs may be efficiently degraded by MGL in these two structures irrespective of its target. 2-AG around presynaptic terminals of CFs and GABAergic

axons may be degraded similarly to that around PF terminals. Hence, there is no apparent synapse specificity in terms of 2-AG degradation in the ML. It is not clear how extracellular 2-AG is eventually degraded by MGL located in the cytoplasm. One possibility would be that 2-AG is incorporated into membrane, caught by MGL attached to the inner leaflet of the membrane, and then hydrolyzed into arachidonic acid and glycerol. Heterogeneous expression of MGL is also found in other brain regions. In the dentate gyrus, MGL is expressed in astrocytes and in some GABAergic inhibitory terminals of both CB_1 receptor-positive and -negative interneurons (78). By marked contrast, MGL is absent in excitatory mossy cell terminals, although DGLα is abundantly expressed in the spine neck of dentate granule cell (DGC) (78). Each DGC spine was found to be innervated by a single mossy cell terminal and also contacted non-synaptically by other mossy cell terminals (78). This molecular and morphological configuration suggests that 2-AG produced at DGC spine neck is readily accessible to neighboring mossy cell-DGC synapses and to inhibitory synapses nearby. It is interesting to test whether DSE is prolonged in MGL-KO mice at mossy cell-DGC synapses where MGL expression is lacking. MGL is considered to be important for determining the extent of 2-AG diffusion in brain tissues. In the cerebellum, PC

depolarization suppresses the firing rates of neighboring interneurons and reduces inhibitory inputs to PCs (90). These effects are now considered to be mediated by 2-AG released by PC depolarization (91). Thus, 2-AG-mediated retrograde signaling is not strictly synapse-specific but is essentially diffusible and can affect neighboring neurons and synapses within a certain distance from the site of 2-AG production. Spatial arrangement of DGLα, CB_1 receptor and MGL is unique to each brain area and, therefore, the magnitude and the extent of diffusion of 2-AG signaling are different. The results of the present study suggest that MGL regulates 2-AG signaling rather broadly within a certain range of neural tissue, although MGL expression is heterogeneous and limited to a subset of nerve terminals and astrocytes.

General discussion

Since the discovery of endocannabinoid as a retrograde messenger (78), extensive research has been performed for elucidation of endocannabinoid mobilization from activated neurons as summarized in the general introduction section. In the present study, I have demonstrated that 2-AG produced through DGLα exclusively mediates retrograde synaptic suppression (part 1) (Figure 24). I have also disclosed that 2-AG is degraded in a synapse type-independent manner by MGL present in subsets of presynaptic terminals and astrocytes after inducing retrograde synaptic suppression (part 2) (Figure 25).

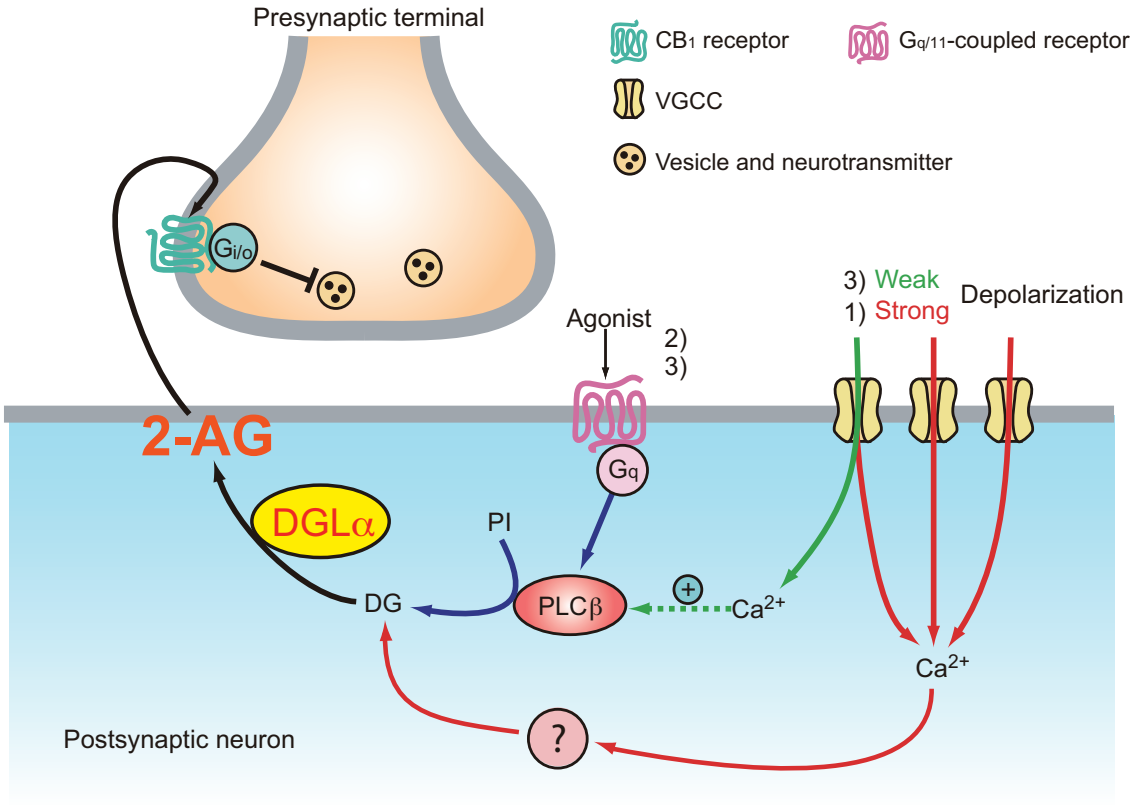

Figure 24. 2-AG produced by DGLα mediates retrograde signaling.

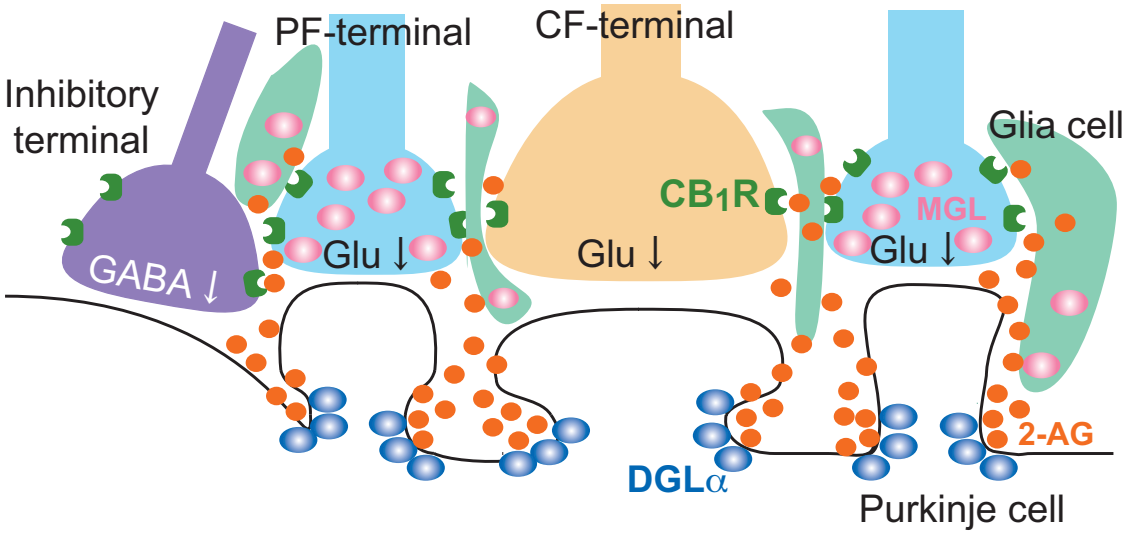

Figure 25. 2-AG is degraded by MGL in synapse non-specific manner.

Thus, basic mechanisms for 2-AG-mediated retrograde synaptic modulation have largely been clarified. However, many unresolved matters still remain. For example, it has not been clarified how 2-AG is carried from postsynaptic neurons to presynaptic CB_1 receptor. Several reports suggest that AEA and 2-AG are carried by transporters (37, 92-95), but these molecules have not been characterized. It also remains unsolved how elevation of intracellular Ca^{2+} alone can produce 2-AG (Ca^{2+}-driven ER) to cause DSI/DSE. A certain type of PLC that is activated by Ca^{2+} elevation alone and produces diacylglycerol has been considered to be involved. Since biochemical data indicate that PLCδ can be activated by Ca^{2+} elevation alone, Hashimototani et al. examined whether this PLC subtype is involved in DSI by using mice that lack one of the three PLCδ isoforms (δ1, δ3 and δ4) (35). However, all of the three knockout mice exhibited normal DSI in cultured hippocampal neurons. A recent report argues that cytosolic phospholipase A2α (cPLA2α) mediates DSE at PF-PC synapses based on the observations that DSE was absent in cPLA2α knockout mice and application of arachidonic acid restored DSE in cPLA2α knockout cerebellum. Furthermore the authors showed that application of MGL into PCs inhibited DSE. These results suggest that cPLA2α-arachidonic acid pathway is required and 2-AG is produced downstream

of arachidonic acid (96). These results are in striking contrast to the results of the present studies that DSE is abolished in PCs of DGLα knockout mice. Moreover, several previous studies demonstrated that DSE was abolished by DGL inhibitors (35). The reasons for this discrepancy are currently unclear, but they showed neither the reduction of basal 2-AG content in cPLA2α knockout cerebellum nor production of 2-AG following cPLA2α activation in WT cerebellum. Careful studies are needed to clarify whether pathways for 2-AG production not involving DGLα exist in neurons or not.

Tonic activation of CB_1 receptor has been shown to induce alteration of surface trafficking and surface expression of CB_1 receptor (97, 98). In MGL-KO mice, CB_1 receptor expression was reported to be reduced in several brain areas presumably due to the marked elevation of basal 2-AG contents (71). In the cerebellum, Zhong et al. (75) showed that magnitude of PF-DSE was significantly decreased and the suppression of PF-PC synapses induced by the CB_1 agonist WIN55, 212-2 was diminished in MGL-KO mice at P 20–25. They suggest that accumulation of 2-AG may induce desensitization of CB_1 receptor in the cerebellum. However, I could not find obvious changes in the magnitude of WIN55, 212-2 (1 μM, 3 μM, 10 μM)-induced suppression

and paired-pulse ratio at PF-PC synapses in MGL-KO mice at P12-16, indicating that CB_1 receptor sensitivity and basic properties at PF-PC synapses are not significantly altered in the MGL-KO cerebellum. The apparent discrepancy between the results by Zhong et al. and those of the present study is presumably ascribed to the difference in the mouse age. Zhong et al. also analyzed younger mice and showed that the magnitude of PF-DSE was not decreased in MGL-KO mice at P10-14. These results suggest that the down regulation of CB_1 receptor is not apparent until around P16 but becomes obvious after P20.

In part 2, I have demonstrated that 2-AG-mediated retrograde signaling is regulated by MGL in a synapse non-specific manner in the cerebellum. What would be the functional relevance of the MGL-dependent regulation of 2-AG signaling? In the hippocampus of MGL-KO mice, the basal level of 2-AG is markedly increased (71) and theta burst stimulation- induced long-term potentiation (LTP) was reported to be enhanced in the CA1 region (74). The amplitude of IPSCs recorded from CA1 pyramidal neurons was shown to be increased by CB_1 receptor antagonist in MGL-KO mice, suggesting that inhibitory synaptic transmission to pyramidal cells is tonically suppressed by ambient 2-AG through CB_1 receptors in the hippocampus of MGL-KO

mice. The reduced inhibition might be a cause for the facilitation of LTP induction in MGL-KO mice. The enhanced LTP might account for improved performance in novel object recognition and Morris water maze in MGL-KO mice (74). As for the cerebellum, LTD at PF-PC synapses (PF-LTD) has been reported to involve endocannabinoid signaling (33). Since PF-LTD is considered to be a cellular basis of certain forms of motor learning (99), it is possible that PF-LTD may be altered and cerebellum-dependent motor learning may be affected in MGL-KO mice. Future work to address these issues should help us understand the roles of MGL and 2-AG signaling in cerebellar function.

Acknowledgment

I would like to express my sincere gratitude to Professor Masanobu Kano for supervising me during the graduate course.

I am deeply grateful to Professor Kouichi Hashimoto, Dr Yuki Hashimotodani and Dr Kazuo Kitamura for warm and helpful advices.

I also thank Dr. Maya Yamazaki, Dr. Manabu Abe and Professor Kenji Sakimura for the generation of DGLα-KO, DGLβ-KO, MGL-GC specific-KO and MGL-KO mice and helpful discussions; Dr. Motokazu Uchigashima and Professor Masahiko Watanabe for the morphological data and helpful discussions; Dr. Yoshihiro Kita and Professor Takao Shimizu for HPLC analysis and helpful discussions.

Thanks to labolatory members for kind helps and supports.

Reference

1. Gaoni Y & Mechoulam R (1971) Isolation, structure and partial synthesis of an active consistent of hashish. *J Am Chem Soc* 93(1):217-224.
2. Matsuda LA, Lolait SJ, Brownstein MJ, Young AC, & Bonner TI (1990) Structure of a cannabinoid receptor and functional expression of the cloned cDNA. *Nature* 346(6284):561-564.
3. Munro S, Thomas KL, & Abu-Shaar M (1993) Molecular characterization of a peripheral receptor for cannabinoids. *Nature* 365(6441):61-65.
4. Decance WA, Hanus L, Breuer A, Pertwee RG, Stevenson LA, Griffin G, Gibson D, Mandelbaum A, Etinger A, Mechoulam R (1992) Isolation and structure of a brain constituent that binds to the cannabinoid receptor.*Science* 258 (5090):1946-1949.
5. Mechoulam R, Ben-Shabat S, Hanus L, Ligumsky M, Kaminski NE, Schatz AR, Gopher A, Almog S, Martin BR, Compton DRPertwee RG, Griffin G, Bayewitch M, Barg J, Vogel Z. (1995) Identification of an endogenous 2-monoglyceride, present in canine gut, that binds to cannabinoid receptors. *Biochem Pharmacol* 50(1):83-90.
6. Sugiura T, Kondo S, Sukagawa A, Nakane S, Shinoda A, Itoh K, Yamashita A, Waku K (1995) 2-Arachidonoylglycerol: a possible endogenous cannabinoid receptor ligand in brain. *Biochem Biophys Res Commun* 215(1):89-97.
7. Llano I, Leresche N, & Marty A (1991) Calcium entry increases the sensitivity of cerebellar Purkinje cells to applied GABA and decreases inhibitory synaptic currents. *Neuron* 6(4):565-574.
8. Kreitzer AC & Regehr WG (2001) Retrograde inhibition of presynaptic calcium influx by endogenous cannabinoids at excitatory synapses onto Purkinje cells. *Neuron* 29(3):717-727.
9. Ohno-Shosaku T, Maejima T, & Kano M (2001) Endogenous cannabinoids mediate retrograde signals from depolarized postsynaptic neurons to presynaptic terminals. *Neuron* 29(3):729-738

10. Wilson RI & Nicoll RA (2001) Endogenous cannabinoids mediate retrograde signalling at hippocampal synapses. *Nature* 410(6828):588-592.
11. Kano M, Ohno-Shosaku T, Hashimotodani Y, Uchigashima M, & Watanabe M (2009) Endocannabinoid-mediated control of synaptic transmission. *Physiol Rev* 89(1):309-380.
12. Hampson RE, Evans GJ, Mu J, Zhuang SY, King VC, Childers SR, Deadwyler SA (1995) Role of cyclic AMP dependent protein kinase in cannabinoid receptor modulation of potassium "A-current" in cultured rat hippocampal neurons. *Life Sci* 56(23-24):2081-2088.
13. Mackie K, Lai Y, Westenbroek R, & Mitchell R (1995) Cannabinoids activate an inwardly rectifying potassium conductance and inhibit Q-type calcium currents in AtT20 cells transfected with rat brain cannabinoid receptor. *J Neurosci* 15(10):6552-6561.
14. Twitchell W, Brown S, & Mackie K (1997) Cannabinoids inhibit N- and P/Q-type calcium channels in cultured rat hippocampal neurons. *J Neurophysiol* 78(1):43-50.
15. Mu J, Zhuang SY, Kirby MT, Hampson RE, & Deadwyler SA (1999) Cannabinoid receptors differentially modulate potassium A and D currents in hippocampal neurons in culture. *J Pharmacol Exp Ther* 291(2):893-902.
16. Schweizer P (2000) Cnnabinoid decrease the K(+) M-current in hippocampal CA1 neurons. *J Neurosci* 20(1):51-58.
17. Cadas H, di Tomaso E, & Piomelli D (1997) Occurrence and biosynthesis of endogenous cannabinoid precursor, N-arachidonoyl phosphatidylethanolamine, in rat brain. *J Neurosci* 17(4):1226-1242.
18. Okamoto Y, Wang J, Morishita J, & Ueda N (2007) Biosynthetic pathways of the endocannabinoid anandamide. *Chem Biodivers* 4(8):1842-1857.
19. Blankman JL, Simon GM, & Cravatt BF (2007) A comprehensive profile of brain enzymes that hydrolyze the endocannabinoid 2-arachidonoylglycerol. *Chem Biol* 14(12):1347-1356.
20. Ohno-Shosaku T, Hashimotodani Y, Ano M, Takeda S, Tsubokawa H,

Kano M (2007) Endocannabinoid signalling triggered by NMDA receptor-mediated calcium entry into rat hippocampal neurons. *J Physiol* 584(Pt 2):407-418.

21. Maejima T, Ohno-Shosaku T, & Kano M (2001) Endogenous cannabinoid as a retrograde messenger from depolarized postsynaptic neurons to presynaptic terminals. *Neurosci Res* 40(3):205-210.
22. Fukudome Y, Ohno-Shosaku T, Matsui M, Omori Y, Fukaya M, Tsubokawa H, Taketo MM, Watanabe M, Manabe T, Kano M (2004) Two distinct classes of muscarinic action on hippocampal inhibitory synapses: M2-mediated direct suppression and M1/M3-mediated indirect suppression through endocannabinoid signalling. *Eur J Neurosci* 19(10):2682-2692.
23. Best AR & Regehr WG (2008) Serotonin evokes endocannabinoid release and retrogradely suppresses excitatory synapses. *J Neurosci* 28(25):6508-6515.
24. Haj-Dahmane S & Shen RY (2005) The wake-promoting peptide orexin-B inhibits glutamatergic transmission to dorsal raphe nucleus serotonin neurons through retrograde endocannabinoid signaling. *J Neurosci* 25(4):896-905.
25. Oliet SH, Baimoukhametova DV, Piet R, & Bains JS (2007) Retrograde regulation of GABA transmission by the tonic release of oxytocin and endocannabinoids governs postsynaptic firing. *J Neurosci* 27(6):1325-1333.
26. Hashimotodani Y, Ohno-Shosaku T, Tsubokawa H, Ogata H, Emoto K, Maejima T, Araishi K, Shin HS, Kano M (2005) Phospholipase Cbeta serves as a coincidence detector through its Ca^{2+} dependency for triggering retrograde endocannabinoid signal. *Neuron* 45(2):257-268.
27. Maejima T, Oka S, Hashimotodani Y, Ohno-Shosaku T, Aiba A, Wu D, Waku K, Sugiura T, Kano M (2005) Synaptically driven endocannabinoid release requires Ca^{2+}-assisted metabotropic glutamate receptor subtype 1 to phospholipase Cbeta4 signaling cascade in the cerebellum. *J Neurosci* 25(29):6826-6835.
28. Narushima M, Uchigashima M, Fukaya M, Matsui M, Manabe T,

Hashimoto K, Watanabe M, Kano M (2007) Tonic enhancement of endocannabinoid-mediated retrograde suppression of inhibition by cholinergic interneuron activity in the striatum. *J Neurosci* 27(3):496-506.

29. Kim J, Isokawa M, Ledent C, & Alger BE (2002) Activation of muscarinic acetylcholine receptors enhances the release of endogenous cannabinoids in the hippocampus. *J Neurosci* 22(23):10182-10191.
30. Galante M & Diana MA (2004) Group I metabotropic glutamate receptors inhibit GABA release at interneuron-Purkinje cell synapses through endocannabinoid production. *J Neurosci* 24(20):4865-4874.
31. Jung KM, Mangieri R, Stapleton C, Kin J, Fegley D, Wallace M, Mackie K, Piomelli D (2005) Stimulation of endocannabinoid formation in brain slice cultures through activation of group I metabotropic glutamate receptors. *Mol Pharmacol* 68(5):1196-1202 .
32. Melis M, Pistis M, Perra S, Muntoni AL, Pillolla G, Gessa GL (2004) Endocannabinoids mediate presynaptic inhibition of glutamatergic transmission in rat ventral tegmental area dopamine neurons through activation of CB1 receptors. *J Neurosci* 24(1):53-62.
33. Safo PK & Regehr WG (2005) Endocannabinoids control the induction of cerebellar LTD. *Neuron* 48(4):647-659.
34. Chevaleyre V & Castillo PE (2003) Heterosynaptic LTD of hippocampal GABAergic synapses: a novel role of endocannabinoids in regulating excitability. *Neuron* 38(3):461-472.
35. Hashimotodani Y, Ohno-Shosaku T, Maejima T, Fukami K, & Kano M (2008) Pharmacological evidence for the involvement of diacylglycerol lipase in depolarization-induced endocanabinoid release. *Neuropharmacology* 54(1):58-67.
36. Uchigashima M, Narushima M, Fukaya M, Katona I, Kano M, Watanabe M (2007) Subcellular arrangement of molecules for 2-arachidonoyl-glycerol-mediated retrograde signaling and its physiological contribution to synaptic modulation in the striatum. *J Neurosci* 27(14):3663-3676.

37. Bisogno T, Howell F, Williams G, Minassi A, Cascio MG, Ligresti A, Matias I, SchianopMoriello A, Paul P, Williams EJ, Gangadharan U, Hobbs C, Di Marzo V, Doherty P (2003) Cloning of the first sn1-DAG lipases points to the spatial and temporal regulation of endocannabinoid signaling in the brain. *J Cell Biol* 163(3):463-468.
38. Mishina M & Sakimura K (2007) Conditional gene targeting on the pure C57BL/6 genetic background. *Neurosci Res* 58(2):105-112.
39. Fuse T, Kanai Y, Kanai-Azuma M, Suzuki M, Makamura K, Mori H, Hayashi Y, Mishina M (2004) Conditional activation of RhoA suppresses the epithelial to mesenchymal transition at the primitive streak during mouse gastrulation. *Biochem Biophys Res Commun* 318(3):665-672.
40. Kano M, Hashimoto K, Chen C, Abellovich A, Kurihara H, Watanabe M, Inoue Y, Tonegawa S (1995) Impaired synapse elimination during cerebellar development in PKC gamma mutant mice. *Cell* 83(7):1223-1231.
41. Hashimotodani Y, Ohno-Shosaku T, & Kano M (2007) Presynaptic monoacylglycerol lipase activity determines basal endocannabinoid tone and terminates retrograde endocannabinoid signaling in the hippocampus. *J Neurosci* 27(5):1211-1219.
42. Ohno-Shosaku T, Shosaku J, Tsubokawa H, & Kano M (2002) Cooperative endocannabinoid production by neuronal depolarization and group I metabotropic glutamate receptor activation. *Eur J Neurosci* 15(6):953-961.
43. Tsubokawa H, Offermanns S, Simon M, & Kano M (2000) Calcium-dependent persistent facilitation of spike backpropagation in the CA1 pyramidal neurons. *J Neurosci* 20(13):4878-4884.
44. Yoshida T, Fukaya M, Uchigashima M, Miura E, Kamiya H, Kano M, Watanabe M (2006) Localization of diacylglycerol lipase-alpha around postsynaptic spine suggests close proximity between production site of an endocannabinoid, 2-arachidonoyl-glycerol, and presynaptic cannabinoid CB1 receptor. *J Neurosci* 26(18):4740-4751.
45. Tanaka J, Nakagawa S, Kushiya E, Yamasaki M, Fukaya M, Iwanaga

T, Simon MI, Sakimura K, Kano M, Watanabe M (2000) Gq protein alpha subunits Galphaq and Galpha11 are localized at postsynaptic extra-junctional membrane of cerebellar Purkinje cells and hippocampal pyramidal cells. *Eur J Neurosci* 12(3):781-792.

46. Fukaya M, Uchigashima M, Nomura S, Hasegawa Y, Kikuchi H, Watanabe M (2008) Predominant expression of phospholipase Cbeta1 in telencephalic principal neurons and cerebellar interneurons, and its close association with related signaling molecules in somatodendritic neuronal elements. *Eur J Neurosci* 28(9):1744-1759.
47. Nakamura M, Sato K, Fukaya M, Araishi K, Aiba A, Kano M, Watanabe M (2004) Signaling complex formation of phospholipase Cbeta4 with metabotropic glutamate receptor type 1alpha and 1,4,5-trisphosphate receptor at the perisynapse and endoplasmic reticulum in the mouse brain. *Eur J Neurosci* 20(11):2929-2944.
48. Brown SP, Brenowitz SD, & Regehr WG (2003) Brief presynaptic bursts evoke synapse-specific retrograde inhibition mediated by endogenous cannabinoids. *Nat Neurosci* 6(10):1048-1057.
49. Batchelor AM & Garthwaite J (1997) Frequency detection and temporally dispersed synaptic signal association through a metabotropic glutamate receptor pathway. *Nature* 385(6611):74-77.
50. Narushima M, Hashimoto K, & Kano M (2006) Endocannabinoid-mediated short-term suppression of excitatory synaptic transmission to medium spiny neurons in the striatum. *Neurosci Res* 54(3):159-164.
51. Chevaleyre V, Takahashi KA, & Castillo PE (2006) Endocannabinoid-mediated synaptic plasticity in the CNS. *Annu Rev Neurosci* 29:37-76.
52. Hashimotodani Y, Ohno-Shosaku T, & Kano M (2007) Endocannabinoids and synaptic function in the CNS. *Neuroscientist* 13(2):127-137.
53. Heifets BD & Castillo PE (2009) Endocannabinoid signaling and long-term synaptic plasticity. *Annu Rev Physiol* 71:283-306.
54. Katona I & Freund TF (2008) Endocannabinoid signaling as a

synaptic circuit breaker in neurological disease. *Nat Med* 14(9):923-930.

55. Bisogno T, Ligresti A, & Di Marzo V (2005) The endocannabinoid signalling system: biochemical aspects. *Pharmacol Biochem Behav* 81(2):224-238.
56. Sugiura T, Kishimoto S, Oka S, & Gokoh M (2006) Biochemistry, pharmacology and physiology of 2-arachidonoylglycerol, an endogenous cannabinoid receptor ligand. *Prog Lipid Res* 45(5):405-446.
57. Vandevoorde S & Lambert DM (2007) The multiple pathways of endocannabinoid metabolism: a zoom out. *Chem Biodivers* 4(8):1858-1881.
58. Katona I, Urban GM, Wallace M, Ledent C, Jung KM, Piomelli D, Mackie K, Freund TF (2006) Molecular composition of the endocannabinoid system at glutamatergic synapses. *J Neurosci* 26(21):5628-5637.
59. Lafourcade M, Elezgarai I, Mato S, Bakiri Y, Grandes P, Manzoni OJ (2007) Molecular components and functions of the endocannabinoid system in mouse prefrontal cortex. *PLoS One* 2(8):e709.
60. Hashimotodani Y, Ohno-Shosaku T, & Kano M (2007) Ca(2+)-assisted receptor-driven endocannabinoid release: mechanisms that associate presynaptic and postsynaptic activities. *Curr Opin Neurobiol* 17(3):360-365.
61. Katona I, Sperlagh B. Slk A, Kafaivi A, Vizi ES, Mackie K, Freund TF (1999) Presynaptically located CB1 cannabinoid receptors regulate GABA release from axon terminals of specific hippocampal interneurons. *J Neurosci* 19(11):4544-4558.
62. Kawamura Y, Fukaya M, Maejima T, Yoshida T, Miura E, Watanabe M, Ohno-Shosaku T, Kano M (2006) The CB1 cannabinoid receptor is the major cannabinoid receptor at excitatory presynaptic sites in the hippocampus and cerebellum. *J Neurosci* 26(11):2991-3001.
63. Suarez J, Bermudez-silva FJ, Mackie K, Ledent C, Zimmer A, Cravatt BF, de Fonseca FR (2008) Immunohistochemical description of the

endogenous cannabinoid system in the rat cerebellum and functionally related nuclei. *J Comp Neurol* 509(4):400-421.

64. Zhao Y, Rubio ME, & Tzounopoulos T (2009) Distinct functional and anatomical architecture of the endocannabinoid system in the auditory brainstem. *J Neurophysiol* 101(5):2434-2446.
65. Harkany T, Guzman M, Galve-Roperh I, Berghuis P, Devi LA, Mackie K (2007) The emerging functions of endocannabinoid signaling during CNS development. *Trends Pharmacol Sci* 28(2):83-92.
66. Iversen L (2003) Cannabis and the brain. *Brain* 126(Pt 6):1252-1270.
67. Lujan R, Nusser Z, Roberts JD, Shigemoto R, & Somogyi P (1996) Perisynaptic location of metabotropic glutamate receptors mGluR1 and mGluR5 on dendrites and dendritic spines in the rat hippocampus. *Eur J Neurosci* 8(7):1488-1500.
68. Yoshida T, Uchigashima M, Yamasaki M, Katona I, Yamazaki M, Sakimura K, Kano M, Yoshioka M, Watanabe M (2011) Unique inhibitory synapse with particularly rich endocannabinoid signaling machinery on pyramidal neurons in basal amygdaloid nucleus. *Proc Natl Acad Sci U S A* 108(7):3059-3064.
69. Yoshida A, Hama S, Nakashima K, & Kondo A (2011) Water activity dependence of performance of surface-displayed lipase in yeast cells: a unique water requirement for enzymatic synthetic reaction in organic media. *Enzyme Microb Technol* 48(4-5):334-338.
70. Chanda PK, Gao Y, Mark L, Btesh J, Strassie BW, Lu P, Piesia MJ, Zhang MY, Bingham B, Uveges A, Kowal D, Garbe D, Kouranova EV, Ring RH, Bates B, Pangaios MN, Kennedy JD, Whiteside GT, Samad TA (2010) Monoacylglycerol lipase activity is a critical modulator of the tone and integrity of the endocannabinoid system. *Mol Pharmacol* 78(6):996-1003.
71. Schlosburg JE, Blankman JL, Long JZ, Nomura DK, Pan B, Kinsey SG, Nguyen PT, Ramesh D, Booker L, Burston JJ, Thomas EA, Selley DE, Sim-Selley LJ, Liu QS, Lichtman AH, Cravatt BF (2010) Chronic monoacylglycerol lipase blockade causes functional antagonism of the endocannabinoid system. *Nat Neurosci* 13(9):1113-1119.

72. Pan B, Wang W, Long JZ, Sun D, Hillard CJ, Cravatt BF, Liu QS (2009) Blockade of 2-arachidonoylglycerol hydrolysis by selective monoacylglycerol lipase inhibitor 4-nitrophenyl 4-(dibenzo[d][1,3]dioxol-5-yl(hydroxy)methyl)piperidine-1-carboxylate (JZL184) Enhances retrograde endocannabinoid signaling. *J Pharmacol Exp Ther* 331(2):591-597.
73. Straiker A, Hu SS, Long JZ, Arnold A, Wager-Miller J, Cravatt BF, Mackie K (2009) Monoacylglycerol lipase limits the duration of endocannabinoid-mediated depolarization-induced suppression of excitation in autaptic hippocampal neurons. *Mol Pharmacol* 76(6):1220-1227.
74. Pan B, Wang W, Zhong P, Blankman JL, Cravatt BF, Liu QS (2011) Alterations of endocannabinoid signaling, synaptic plasticity, learning, and memory in monoacylglycerol lipase knock-out mice. *J Neurosci* 31(38):13420-13430.
75. Zhong P, Pan B, Gao XP, Blankman JL, Cravatt BF, Liu QS (2011) Genetic deletion of monoacylglycerol lipase alters endocannabinoid-mediated retrograde synaptic depression in the cerebellum. *J Physiol* 589(Pt 20):4847-4855.
76. Dinh TP, Carpenter D, Leslie FM, Freund TF, Katona L, Sensi SL, Kathuria S, Piomelli D (2002) Brain monoglyceride lipase participating in endocannabinoid inactivation. *Proc Natl Acad Sci U S A* 99(16):10819-10824.
77. Gulyas AI, Cravatt BF, Bracey MH, Dinh TP, Piomelli D, Boscia F, Freund TF (2004) Segregation of two endocannabinoid-hydrolyzing enzymes into pre- and postsynaptic compartments in the rat hippocampus, cerebellum and amygdala. *Eur J Neurosci* 20(2):441-458.
78. Uchigashima M, Yamazaki M, Yamasaki M, Tanimura A, Sakimura K, Kano M, Watanabe M (2011) Molecular and morphological configuration for 2-arachidonoylglycerol-mediated retrograde signaling at mossy cell-granule cell synapses in the dentate gyrus. *J Neurosci* 31(21):7700-7714.

79. Tanimura A, Yamazaki M, Hashimotodani Y, Uchigashima M, Kawata S, Abe M, Kita Y, Hashimoto K, Shimizu T, Watanabe M, Sakimura K, Kano M (2010) The endocannabinoid 2-arachidonoylglycerol produced by diacylglycerol lipase alpha mediates retrograde suppression of synaptic transmission. *Neuron* 65(3):320-327.
80. Miyazaki T, Yamasaki M, Hashimoto K, Yamazaki M, Abe M, Usui H, Kano M, Sakimura K, Watanabe M (2012) Cav2.1 in cerebellar Purkinje cells regulates competitive excitatory synaptic wiring, cell survival, and cerebellar biochemical compartmentalization. *J Neurosci* 32(4):1311-1328.
81. Maejima T, Hashimoto K, Yoshida T, Aiba A, & Kano M (2001) Presynaptic inhibition caused by retrograde signal from metabotropic glutamate to cannabinoid receptors. *Neuron* 31(3):463-475.
82. Yamamoto N, Kurotani T, & Toyama K (1989) Neural connections between the lateral geniculate nucleus and visual cortex in vitro. *Science* 245(4914):192-194.
83. Torashima T, Okoyama S, Nishizaki T, & Hirai H (2006) In vivo transduction of murine cerebellar Purkinje cells by HIV-derived lentiviral vectors. *Brain Res* 1082(1):11-22.
84. Fremeau RT, Jr., Troyer MD, Pahner I, Nygaard GO, Tran CH, Reimer RJ, Bellocchio EE, Storm-Mathisen J, Edwards RH (2001) The expression of vesicular glutamate transporters defines two classes of excitatory synapse. *Neuron* 31(2):247-260.
85. Yamada K, Fukaya M, Shibata T, Kurihara H, Tanaka K, Inoue Y, Watanabe M (2000) Dynamic transformation of Bergmann glial fibers proceeds in correlation with dendritic outgrowth and synapse formation of cerebellar Purkinje cells. *J Comp Neurol* 418(1):106-120.
86. Hashimoto K, Ichikawa R, Kitamura K, Watanabe M, & Kano M (2009) Translocation of a "winner" climbing fiber to the Purkinje cell dendrite and subsequent elimination of "losers" from the soma in developing cerebellum. *Neuron* 63(1):106-118.
87. Roth A & Hausser M (2001) Compartmental models of rat cerebellar

Purkinje cells based on simultaneous somatic and dendritic patch-clamp recordings. *J Physiol* 535(Pt 2):445-472.

88. Long JZ, Li W, Booker L, Burston JJ, Kinsey SG, Schlosburg JE, Pavon FJ, Serrano AM, Selley DE, Parsons LH, Lichtman AH, Cravatt BF (2009) Selective blockade of 2-arachidonoylglycerol hydrolysis produces cannabinoid behavioral effects. *Nat Chem Biol* 5(1):37-44.
89. Gao Y, Vasilyev DV, Goncalves MB, Howell FV, Hobbs C, Reisenberg M, Shen R, Zhang MY, Strassle BW, Lu P, Mark L, Piesia MJ, Deng K, Kouranova EV, Ring RH, Whiteside GT, Bates B, Waish FS, Williams G, Pangalos MN, Samad TA, Doherty P (2010) Loss of retrograde endocannabinoid signaling and reduced adult neurogenesis in diacylglycerol lipase knock-out mice. *J Neurosci* 30(6):2017-2024.
90. Vincent P & Marty A (1993) Neighboring cerebellar Purkinje cells communicate via retrograde inhibition of common presynaptic interneurons. *Neuron* 11(5):885-893.
91. Kreitzer AC, Carter AG, & Regehr WG (2002) Inhibition of interneuron firing extends the spread of endocannabinoid signaling in the cerebellum. *Neuron* 34(5):787-796.
92. Fegley D, Kathuria S, Mercier R, Li C, Goutopoulos A, Makriyannis A, Piomelli D (2004) Anandamide transport is independent of fatty-acid amide hydrolase activity and is blocked by the hydrolysis-resistant inhibitor AM1172. *Proc Natl Acad Sci U S A* 101(23):8756-8761.
93. Ligresti A, Morera E, Van Der Stelt M, Monory K, Lutz B, Ortar G, Di Marzo V (2004) Further evidence for the existence of a specific process for the membrane transport of anandamide. *Biochem J* 380(Pt 1):265-272.
94. Beltramo M & Piomelli D (2000) Carrier-mediated transport and enzymatic hydrolysis of the endogenous cannabinoid 2-arachidonylglycerol. *Neuroreport* 11(6):1231-1235.
95. Piomelli D, Beltramo M, Glasnapp S, Lin SY, Goutopoulos A, Xie XQ, Makriyannis A (1999) Structural determinants for recognition and translocation by the anandamide transporter. *Proc Natl Acad Sci U S*

A 96(10):5802-5807.

96. Wang DJ, Yang D, Su LD, Xie YJ, Zhou L, Sun CL, Wang XX, Zhou L, Shen Y (2012) Cytosolic Phospholipase A(2) alpha/Arachidonic Acid Signaling Mediates Depolarization-Induced Suppression of Excitation in the Cerebellum. *PLoS One* 7(8):e41499.
97. Wu DF, Yang LQ, Goschke A, Stumm R, Brandenburg LO, Liang YJ, Hollt V, Koch T (2008) Role of receptor internalization in the agonist-induced desensitization of cannabinoid type 1 receptors. *J Neurochem* 104(4):1132-1143.
98. Mikasova L, Groc L, Choquet D, & Manzoni OJ (2008) Altered surface trafficking of presynaptic cannabinoid type 1 receptor in and out synaptic terminals parallels receptor desensitization. *Proc Natl Acad Sci U S A* 105(47):18596-18601.
99. Ito M (2001) Cerebellar long-term depression: characterization, signal transduction, and functional roles. *Physiol Rev* 81(3):1143-1195.